JCTC Journal of Chemical Theory and Computation

pubs.acs.org/JCTC Review

CHARMM-GUI *Membrane Builder*: Past, Current, and Future Developments and Applications

Shasha Feng, Soohyung Park, Yeol Kyo Choi, and Wonpil Im*

Cite This: *J. Chem. Theory Comput.* 2023, 19, 2161−2185 Read Online

ACCESS | Metrics & More | Article Recommendations

ABSTRACT: Molecular dynamics simulations of membranes and membrane proteins serve as computational microscopes, revealing coordinated events at the membrane interface. As G protein-coupled receptors, ion channels, transporters, and membrane-bound enzymes are important drug targets, understanding their drug binding and action mechanisms in a realistic membrane becomes critical. Advances in materials science and physical chemistry further demand an atomistic understanding of lipid domains and interactions between materials and membranes. Despite a wide range of membrane simulation studies, generating a complex membrane assembly remains challenging. Here, we review the capability of CHARMM-GUI *Membrane Builder* in the context of emerging research demands, as well as the application examples from the CHARMM-GUI user community, including membrane biophysics, membrane protein drug-binding and dynamics, protein−lipid interactions, and nano-bio interface. We also provide our perspective on future *Membrane Builder* development.

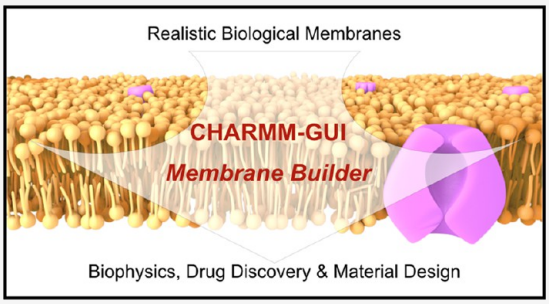

1. INTRODUCTION

Membrane bilayers serve as the matrix to define cell boundaries and anchor biomachineries and signaling pathways.[1] Since the first all-atom molecular dynamics (MD) simulations of lipid membranes and membrane proteins in the late 1980s and early 1990s,[2−6] membrane simulations have played important roles in exploring membrane-related biological processes.[7−12] To name a few, examples include from cholesterol partition in the liquid-order/liquid-disordered phase to lipopolysaccharide (LPS) lipid conformation in Gram-negative bacteria,[13,14] from polyethylenimine gene transfection in a wet lab to lipid nanoparticle (LNP) drug delivery in a patient's body,[15,16] from antimicrobial peptide-membrane interactions in nature to amyloid-β (Aβ) aggregation in Alzheimer's disease,[17,18] and from dopamine transporter drug inhibition to SARS-CoV-2 spike protein recognition.[19,20] A wide range of membrane simulations assist interpretation of virus infection, bacterial defense, disease onset, and drug toxicity, to name just a few.[18,19,21,22]

Accompanying the advance of membrane simulations is the development of experimental techniques to study membrane lateral organizations,[23−25] the arrival of the single-particle cryo-EM era to reveal thousands of membrane protein structures,[26,27] and the maturing of simulation force fields (FFs) and membrane system modeling protocols,[28−30] as well as the shifting focus on membrane proteins as the drug targets.[31] The recent revolution of structure-predicting tools such as AlphaFold2 and RoseTTAFold further adds to the modeling arsenal expanding the scope of protein targets for MD simulations.[32,33] In the pharmaceutical industry, drug discovery is more than ever "structurally enabled", meaning structure-based pharmacology discovery with computer-aided drug discovery (CADD) techniques including docking and free energy calculations.[34]

The CHARMM-GUI cyberinfrastructure is a web-based graphical user interface (GUI) for modeling proteins, glycoconjugates, lipids, ligands, and materials, preparing complex simulation assemblies, and generating the input files for running simulation productions (using Amber, CHARMM, Desmond, GENESIS, GROMACS, LAMMPS, NAMD, OpenMM, and TINKER).[35,36] *Membrane Builder* is one of the central pillars in CHARMM-GUI and is heavily used in membrane simulation studies. It first started with support for three phospholipids in 2007.[37] With continuous development, it now covers more than 670 different lipid or surfactant types in various FFs including CHARMM, Amber, OLPS, Slipids, Drude, Martini, and PACE CG (see Figure 1).[28,38,39] *Membrane Builder* supports all-atom planar bilayer and micelle generation, while CHARMM-GUI *Martini Maker* supports both coarse-grained micelle and vesicle generation. Both

Received: December 8, 2022
Published: April 4, 2023

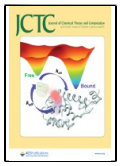

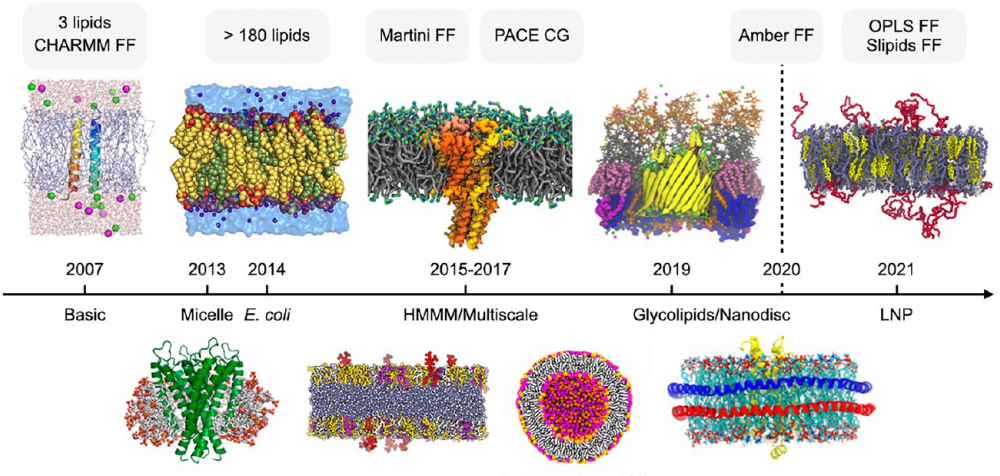

Figure 1. Chronicle of CHARMM-GUI *Membrane Builder* development. From the pioneering stage in 2007 to the recent mature stage, the complexity of model membrane systems and supported resolution, and force fields (FFs, in shaded boxes) have expanded. (Year 2007) A basic simulation system of transmembrane dimer ζ-ζ protein in a DMPC bilayer. Adapted with permission from ref 37. Copyright 2007 PLOS. (Year 2013) A micelle complex of a KcsA K^+ channel. Adapted with permission from ref 60. Copyright 2013 American Chemical Society. (Year 2014) An *Escherichia coli* (*E. coli*) inner membrane model. Adapted with permission from ref 61. Copyright 2014 Wiley Periodicals, Inc. (Years 2015−2017) An HMMM model consisting of truncated lipids and organic solvent in the hydrophobic core. Adapted with permission from ref 62. Copyright 2015 Biophysical Society. A Martini model of mechanosensitive channel of large conductance in a DOPC bilayer. Adapted with permission from ref 63. Copyright 2015 American Chemical Society. (Year 2019) Glycolipids modeling with protein BtuB in *E. coli* outer membrane. Adapted with permission from ref 38. Copyright 2019 American Chemical Society. A nanodisc model of POPC with a GPCR protein. Adapted with permission from ref 64. Copyright 2019 Wiley Periodicals, Inc. (Year 2020) Support of the Amber FFs. (Year 2021) Support of the OPLS and Slipids FFs. An LNP membrane composed of PEGylated diacylglycerol lipid, DSPC, DLin-MC3-DMA, and cholesterol. Adapted with permission from ref 16. Copyright 2021 American Chemical Society. Abbreviations: 1,2-dimyristoyl-phosphatidylcholine (DMPC), 1,2-dioleoyl-phosphatidylcholine (DOPC), 1-palmitoyl-2-oleoyl-phosphocholine (POPC), 1,2-distearoyl-*sn*-glycero-3-phosphocholine (DSPC), dilinoleylmethyl-4-dimethylamino-butyrate (Dlin-MC3-DMA).

Membrane Builder and *Martini Maker* support nanodisc generation. *Membrane Builder* is supported by other functions in CHARMM-GUI such as modeling ligands, glycans, LPS, polymers, nanomaterials, calculating ligand-binding free energy, setting up high-throughput protein−ligand simulations, and applying enhanced sampling techniques.[40−48] These supporting modules enable the modeling of realistic membrane systems for studying the nano-bio interface, biomembrane surface, and drug discovery.

Recently, a realistic mammalian plasma membrane model composed of ∼200,000 lipids with 63 different types in a box of $\sim 71 \times 71 \times 11$ nm^3 was built and simulated for over 40 μs, pushing the boundary of cell-scale simulations.[49] Manually generating large and complex membrane models is time-consuming, prone to errors, and practically impossible. Significant efforts have been made to develop membrane modeling tools by systematically automatizing the workflow. Besides CHARMM-GUI *Membrane Builder*, other membrane building tools include INSANE,[50] Packmol,[51] MembraneEditor,[52] BUMpy,[53] LipidWrapper,[54] and TS2CG,[55] to name just a few. INSANE supports generating a coarse-grained (CG) planar bilayer. Packmol and MembraneEditor support membrane system building with planar, spherical, elliptic, and cylindrical shapes, and MembraneEditor also supports multilayered planar and vesicular membranes. BUMpy supports various shapes of membranes, including torus, semisphere plane, and buckle. LipidWrapper and TS2CG can generate general curved membranes (of arbitrary shapes) by mapping segments of pre-equilibrated membrane or lipids onto triangular surfaces, respectively. AutoPack/cellPack can model membrane-including large-scale cellular environments.[56−58] Nanodisc-Builder can generate nanodisc structures.[59]

In this Review, given the increasing demands for membrane simulations and the growing CHARMM-GUI functionalities, we review the capability of *Membrane Builder* and the innovative applications in the CHARMM-GUI user community. Based on ∼1,600 papers (based on the Web of Science as of September 2022) that cited or used CHARMM-GUI for membrane simulations, we summarize the applications in the following categories: membrane biophysics, membrane protein dynamics, protein−lipid interactions, drug-membrane interactions, and nano-bio interface. We also included some studies that did not use CHARMM-GUI, as they are vivid examples for demonstrating the power of membrane simulations. At the end of this review, we also discuss the future development of *Membrane Builder*, which includes support for bicelle, all-atom vesicle, and multiple copies of components (e.g., membrane proteins, ligands, and even membranes) at desired positions, additional membrane morphologies, nano-bio interfaces, and QM/MM simulations.

2. SUPPORTED MEMBRANE SYSTEMS

Membrane Builder supports the generation of all-atom models of planar monolayer and bilayer membrane, inverse hexagonal phase, micelle, and nanodisc systems (Figure 1). The corresponding CG Martini membranes[30,65] generated by *Martini Maker* in CHARMM-GUI support vesicle generation as well.[66] The generated CG models can be conveniently converted into all-atom models by *All-atom Converter* in *Martini Maker*. In addition, *Membrane Builder* supports the generation of the highly mobile membrane mimetic (HMMM) model,[67] where the lipid hydrophobic tails are truncated and replaced with short hydrocarbons, making the truncated lipids highly mobile.

https://doi.org/10.1021/acs.jctc.2c01246
J. Chem. Theory Comput. 2023, 19, 2161−2185

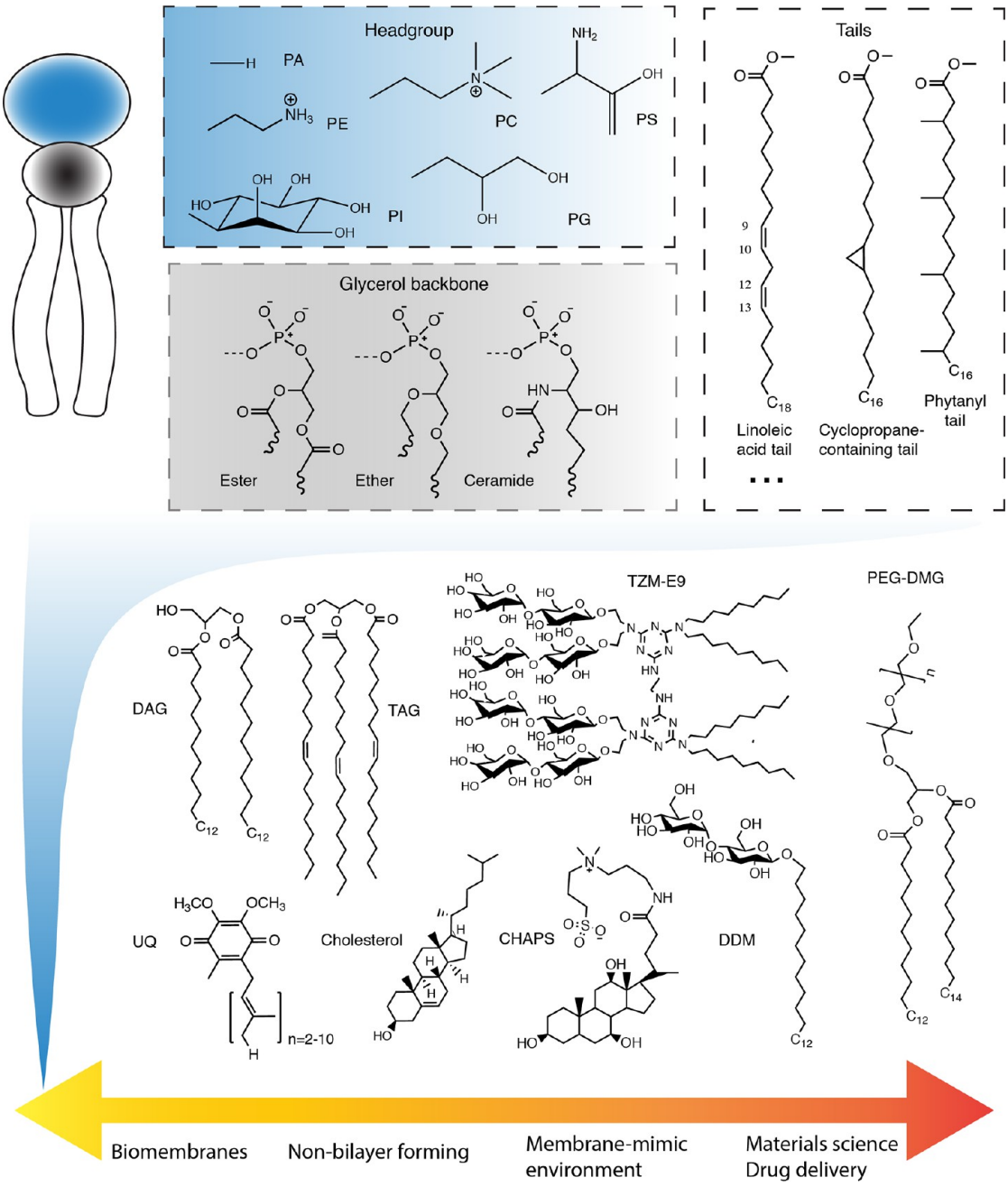

Figure 2. Lipid collection in CHARMM-GUI *Membrane Builder* spans from biomembrane bilayer-forming lipids to nonbilayer forming lipids, detergents for protein sample preparation, and PEG-lipids in LNP membranes for genetic drug delivery. Abbreviations: phosphatidic acid (PA), phosphatidylethanolamine (PE), phosphatidylcholine (PC), phosphatidylserine (PS), phosphatidylinositol (PI), phosphatidylglycerol (PG), diacylglyceride (DAG), triacylglyceride (TAG), ubiquinone (UQ), 3-[(3-cholamidopropyl)dimethylammonio]-1-propanesulfonate (CHAPS), tandem triazine-based maltosides with ethylenediamine linker (TZM-E9), dodecyl-*β*-D-maltoside (DDM), PEGylated myristoyl diglyceride (PEG-DMG).

For a chosen membrane system, *Membrane Builder* provides inputs for various MD engines[68] with compatible FFs including CHARMM, Amber, OPLS, Slipid, and Drude.[69,70] This is one of the unique merits over other tools that usually provide either an initial structure model or inputs for a specific MD engine only. The inputs provided by *Membrane Builder* can be easily modified for user specific purposes. Another important merit of *Membrane Builder* is seamless integration with other modules in CHARMM-GUI. For example, *PDB Reader & Manipulator*,[36,42,71] *Glycolipid Modeler*, and *LPS Modeler*[38] are called by *Membrane Builder* to include peptides, proteins, small molecules, glycolipids, and LPS in a membrane system. Conversely, it can be called by other modules, e.g., a recent study used *Enhanced Sampler* utilizing *Membrane Builder* in generation of inputs for adaptive bias force simulation of Mla protein in a bacterial membrane.[47] Hence, using *Membrane Builder*, one can easily prepare a wide variety of realistic membranes, including components like membrane proteins, nucleic acids, glycoconjugates, drug molecules, and nanoparticles, while adding advanced simulation techniques including steered MD simulation and umbrella sampling.

https://doi.org/10.1021/acs.jctc.2c01246
J. Chem. Theory Comput. 2023, 19, 2161−2185

Here, we provide an overview of the workflow for building membrane systems supported in *Membrane Builder* as well as for CG vesicles in *Martini Maker* (Figure 1). We start with a brief description of the general workflow for building a bilayer, which is applicable to all membrane systems. Then, we outline the unique features for each membrane system. The general workflow involves five steps, originally designed for planar bilayers. In STEP 1, a protein (or protein complex) structure is read in through *PDB Reader & Manipulator* that handles user-specific modifications including protonation states, mutations, post-translational modifications, and disulfide bonds. *PDB Reader & Manipulator* can also handle structures for other types of molecules, such as small ligands, DNA, and RNA. In STEP 2, the orientation of the protein can be adjusted based on user input. In STEP 3, the system size is determined, and lipid-like pseudoatoms are distributed on the membrane surface(s) to assign lipid headgroup positions. In STEP 4, the system components (lipids, solvent, and ions) are generated, and pseudoatoms are replaced by lipids using the replacement method[5,72] from the lipid conformation library for most lipid types or with on-the-fly generated lipids for some lipid types (see section 3 **Supported Lipid Types**). In this stage, the penetration of lipid tails to ring structures in sterols, aromatic side chains, and carbohydrates as well as protein surfaces is checked and remedied if necessary. In STEP 5, the components (protein, membrane, solvent, and ions) are assembled, and the topology and inputs for equilibration (STEP6) and production (STEP7) simulations are generated. For membrane-only systems, the workflow starts from STEP 3.

While the general workflow is common for all supported membrane systems, there are unique features depending on their geometry and types. The planar membrane area (X and Y) is determined based on the cross-sectional protein area (along the membrane normal, Z-axis) and the area per lipid (from the default or user-specified value). In a monolayer generation, an assembled bilayer is converted to a monolayer system by shifting a half unit cell along the Z-axis (with periodic boundary conditions) followed by increasing the Z box size to create hydrophobic tail-air interfaces. In HMMM generation, full-length lipids in an assembled bilayer are truncated (with three to five remaining acyl carbons),[67] and the empty space in the hydrophobic core is filled with pre-equilibrated organic solvents (currently 1,1-dicholroethane).[62] In nanodisc generation, prior to STEP 3, a diameter of circular membrane scaffold protein (MSP) dimer (from 81 to 121 Å) needs to be chosen among 12 supported MSP sequences, and the bilayer region is defined as the area enclosed by the MSP dimer.[64] In micelle generation, the initial geometry is defined as a torus formed by a hemisphere of radius r_m, whose curvature center is shifted by r_p along the lateral dimensions from the Z-axis, where r_m and r_p are the radii of the micelle and the protein, respectively. Pseudoatoms are distributed on the surface of the torus and replaced by detergents.[60] In the generation of a CG vesicle by *Martini Maker*, unlike other tools such as Packmol, MembraneEditor, and BUMpy, exchange of lipids between the inner and outer leaflets as well as that of interior and exterior water molecules is allowed by creating pores in the vesicle.[63] The generated initial vesicle structure (STEP 5) is then subject to equilibration (STEP 6) with gradually decreasing pore radii to obtain the vesicle with closed surfaces for the production run (STEP 7). The conversion of a CG vesicle to an all-atom model is supported by *Martini Maker*. In the generation of an inverse hexagonal phase, lipids are packed around a central water cylinder of radius R, and short hydrocarbons are added to fill the interstitial space in a hexagonal simulation box (along the XY-dimensions).

Asymmetric bilayer systems (planar bilayer and vesicle) can exhibit a mismatch in the surface area between the upper and lower leaflets during simulations, especially when lipid areas are obtained from homogeneous bilayer simulations. To avoid this, the area of each lipid types from the cognate symmetric bilayers can be used.[49,73] For further discussion of this topic, refer to subsection 4.5 **Methods for Generating Asymmetric Bilayers**.

3. SUPPORTED LIPID TYPES

Membrane Builder offers a wide range of supported lipid types, including those found in biological and synthetic membranes and various membrane-like environments.[38] Here, we review the supported lipid types in biological membranes, detergent micelles, and LNP membranes, including those from plasma, yeast, bacterial, archaeal, and plant membranes, as well as ionizable and PEGylated lipids (PEG-lipids) for LNP membranes.[74]

Lipids in biological membranes can be roughly divided into two categories: bilayer-forming and nonbilayer-forming. The former includes phospholipids, while the latter includes sterols diacylglyceride, triacylglyceride, monogalactosyldiacylglycerol, quinones, and squalene.[75] Triacylglycerols consist of three fatty acid chains linked to the glycerol backbone (Figure 2). All membrane lipids share a common structure consisting of a headgroup, backbone, and tails (Figure 2). Headgroups are generally short and polar moieties, while tails are saturated or unsaturated fatty acid chains. Backbones are typically derived from glycerol, sphingosine, or sterol. Therefore, biological membranes are composed of various lipid types whose compositions can vary significantly depending on their origins and environments.[76,77] In addition, fatty acids, lipidated amino acids, and glycopeptides can also be found in membranes.

The distribution of lipids is usually heterogeneous along both the lateral and trans-bilayer dimensions. In plasma membranes, saturated lipids, sphingomyelin, and glycolipids (gangliosides) are major components in the outer (exoplasmic) leaflet, whereas unsaturated lipids and negatively charged lipids (phosphatidylserine (PS), phosphatidic acid (PA), phosphatidylinositol (PI), and phosphatidylinositol phosphate (PIP)) are more abundant in the inner (cytoplasmic) leaflet. Cardiolipins are composed of two phosphatidyl lipids linked to the glycerol backbone and are abundant in the inner leaflet of mitochondrial membranes. In certain bacterial species, membranes can have unique lipids with branched tails[78,79] and/or those with a cyclopropane moiety.[80,81] In particular, the outer leaflet of the outer membrane of Gram-negative bacteria contains LPS where a polysaccharide chain is linked to lipid A with a varying number of tails.[82−84] Archaeal membranes are composed of unique lipids with phytanyl tails and quinone derivatives with various lengths of isoprenoid chains.[85]

In addition to lipids, detergents have also been frequently used in simulations as they dissolve the membrane peptide/protein and form protein-detergent complexes, where a micelle-like detergent belt surrounds the protein transmembrane domain. Conventional detergents with a single tail and headgroup are highly dynamic, resulting in poor stability of the protein-detergent complex. Extensive efforts have been made to improve the stability of the protein-detergent complex, and a few lipidated monosaccharides (n-

https://doi.org/10.1021/acs.jctc.2c01246
J. Chem. Theory Comput. 2023, 19, 2161−2185

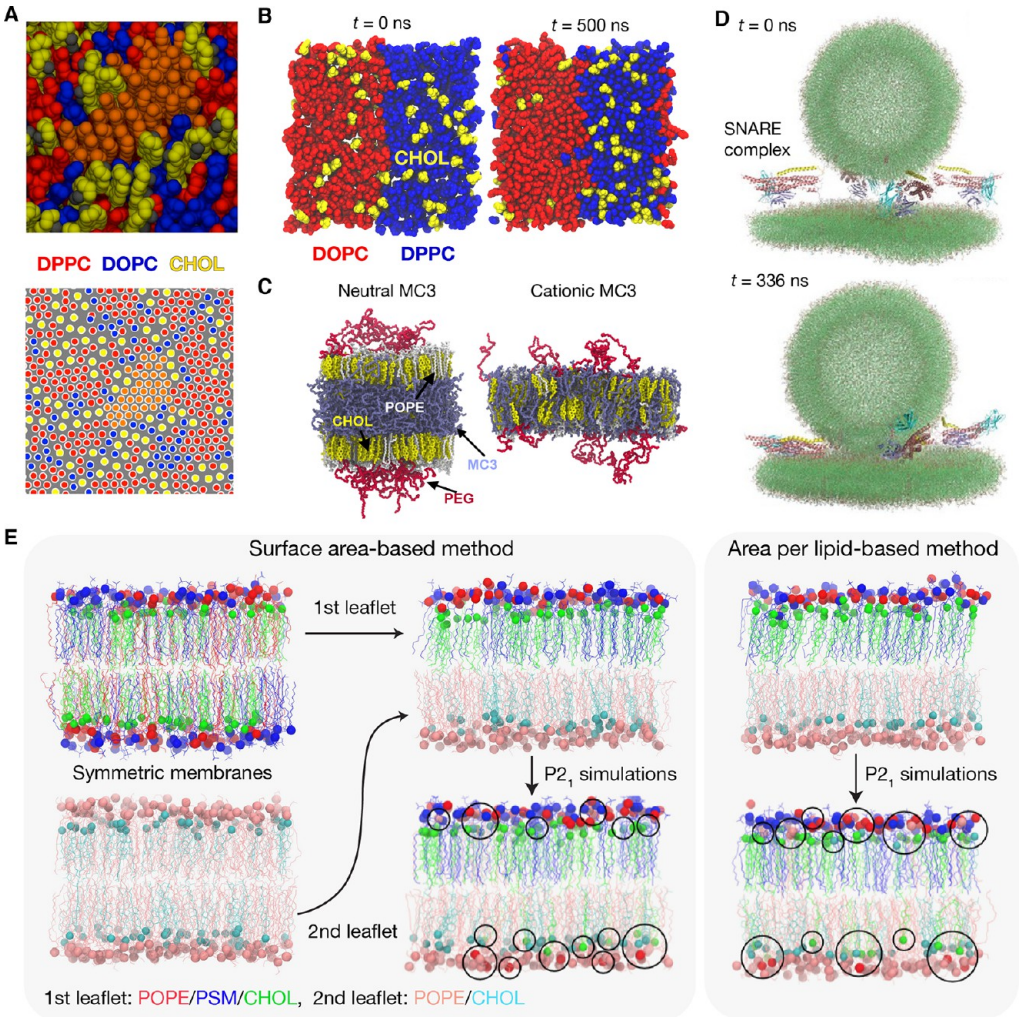

Figure 3. (A) Snapshots of the substructure in Lo domain in a mixed bilayer of DPPC, DOPC, and CHOL (top) and the center of mass of lipid tails (bottom). An area of locally hexagonal order surrounded by CHOL and DOPC is shown in orange. Adapted with permission from ref 116. Copyright 2014 American Chemical Society. (B) CHOL partitioning between a binary bilayer composed of laterally attached DOPC and DPPC bilayers. Randomly distributed CHOLs at t = 0 ns (left) mostly partitioned into DPPC bilayer at t = 500 ns (right). (C) Effects of charge states of the ionizable MC3 lipid on the LNP membrane structure. Neutral MC3 accumulated into the hydrophobic core of the membrane (left), while the positively charged MC3 headgroup remained at the membrane-water interface (right). Adapted with permission from ref 16. Copyright 2021 American Chemical Society. (D) Snapshots of the all-atom simulation of the primed SNARE complex bridging a vesicle and a flat bilayer: initial configuration at t = 0 ns (top) and snapshot at t = 336 ns showing a probable primed state (bottom). Adapted with permission from ref 134. Copyright 2022 eLife. (E) Methods for generating asymmetric bilayers: leaflet surface area matching method (SA), area per lipid-based method (APL), and partial chemical potential matching ($P2_1$) method combined with SA and APL (left and right panels, respectively). During $P2_1$ simulations, POPE and CHOL are allowed to migrate between the leaflets (shown in black circles).

dodecyl-β-D-maltoside (DDM), n-decyl-β-D-maltoside, and n-octyl-β-D-glucoside) and recently developed flexible core bearing detergents (GTMs) and foldable triazine-based maltosides (TZMs) have been shown to be more effective (Figure 2).[86−89] *Membrane Builder* currently supports over 130 different detergents, including these novel GTMs and TZMs.

Another set of important lipid types in LNPs for genetic drug delivery is ionizable (cationic) lipids and PEG-lipids (Figure 2).[90−92] The drug delivery efficacy depends on both the ionizable lipids and PEG-lipids, where the PEG-lipids act as helper lipids along with cholesterols (CHOLs) and phospholipids to stabilize LNPs before uptake into the cytoplasm.[91] When LNPs arrive at the target cells, the PEG chains need to be detached for efficient endocytosis.[93,94] After uptake into the endosome, the endosomal membrane is disrupted by the formation of a nonbilayer structure with anionic lipids (endosomal membrane) and cationic lipids (LNP) at low pH, which drives the release of genetic drugs.[90] Currently, *Membrane Builder* supports six ionizable lipid types (with neutral and cationic forms) with five lipid tails. For PEG-lipids, two backbones, phosphatidylethanolamine (PE) and diacylglycerol, are supported with 50 lipid tails and user-specified PEG chain lengths.

In *Membrane Builder*, the initial conformations of various lipids, fatty acids, *N*-acylated amino acids, detergents, ionizable lipids, and PEG-lipids are chosen from the lipid library and/or generated on-the-fly from user-specified sequences. While the conformations of most predefined lipids, fatty acids, detergents, and ionizable lipids are available in the lipid library, glycolipids, LPS, *N*-acetylated amino acids, and PEG-lipids need to be generated for each user-specified sequence. In on-the-fly generation of glycolipid and LPS, *Glycolipid Modeler*

https://doi.org/10.1021/acs.jctc.2c01246
J. Chem. Theory Comput. 2023, 19, 2161−2185

and *LPS Modeler* in CHARMM-GUI are incorporated because it is not practical to prepare a lipid library for all possible combinations of glycan sequences, core oligosaccharide and O-antigen units, and lipid A from various Gram-negative bacteria, given the combinatorial explosion.[38] An analogous workflow is used in generation of *N*-acetylated amino acids[35] and PEG-lipids[16] due to a similar reason.

4. MEMBRANE BIOPHYSICS

Here, we review the MD simulation applications for membrane biophysics, including membrane domain formations, lipid−lipid interactions, LNP membranes, synaptic vesicle fusion, and the methods for generating asymmetric membrane simulations.

4.1. Membrane Domains. In the current consensus definition, rafts are heterogeneous and dynamic nanodomains (10−200 nm) enriched in sterols, sphingolipids, and certain types of proteins that compartmentalize cellular processes.[95] Larger raft domains can form through protein−protein and protein−lipid interactions.[96,97] Although the definition does not explicitly imply lipid-driven domain formation, in model membranes composed of saturated and unsaturated lipids with CHOL, liquid-ordered (Lo) and liquid-disordered (Ld) domains can coexist.[98−102] These ternary and quaternary models show rich phase behaviors such as critical fluctuations, modulated phases, and a macroscopic phase separation. Similar phase behaviors are also observed in cell-derived membranes,[103,104] suggesting that these model membranes possibly reflect the characteristics of biological membranes.

Accordingly, a large number of computational studies have investigated lipid domains using ternary or quaternary mixture models.[105−113] So far, spontaneous domain formation has been observed only in CG simulations due to slow phase separation kinetics, although a domain formation onset has recently been observed in all-atom simulations.[107,109] While all-atom simulations are still challenging for spontaneous domain formation, the detailed molecular structure of Lo domains has been identified in recent simulations:[114−116] Regions of hexagonally packed saturated lipids are surrounded by unsaturated lipids and CHOLs (Figure 3A), which is later supported by DEER and electron diffraction experiments.[117,118] Hence, it is conceivable that small molecule permeation or membrane protein partitioning in rafts occurs in the regions enriched in unsaturated lipids and CHOLs. Indeed, in a recent simulation study, it was observed that permeation of oxygen and water occurs along the relatively disordered regions in Lo phases.[119]

4.2. Lipid−Lipid Interactions. In lipid-driven domain formation, the preference of CHOL for certain lipid types plays an important role, e.g., the preference for sphingomyelin over phospholipids.[120] CHOL-lipid interactions can be quantified in CHOL exchange experiments between β-cyclodextrin (β-CD) and vesicles with different compositions. β-CD is used as a reference state,[121−124] which elegantly resolves the known issues in direct CHOL exchange between vesicles.[125−127] In computational simulations, CHOL-lipid interactions have been quantitatively characterized by calculating transfer free energies from bilayer to water[128,129] or to β-CD,[130,131] though both are computationally intensive. Recently, an efficient alternative approach, a binary bilayer simulation, has been proposed, where two bilayers are laterally attached, and their interfaces are maintained by soft restraining potentials acting only on selected lipids that diffuse deeply from one bilayer to the other bilayer.[13] In such a setting, as shown in Figure 3B, CHOL (with no imposed restraints) can freely diffuse across bilayers and partition between them without the need of a reference state like β-CD. The binary bilayers can be prepared using slightly modified inputs from *Membrane Builder*, and their efficacy in direct CHOL partitioning simulations was demonstrated by excellent agreement between partition coefficients from simulations and experiments.[13]

4.3. Lipid Nanoparticle Membranes. Recent updates in *Membrane Builder* allow for preparing simulations of realistic LNP membranes composed of ionizable (cationic) lipids and helper lipids such as phospholipids, CHOL, and PEG-lipids.[16] Previously, a few simulation studies have investigated LNP membranes without CHOL and PEG-lipids,[132,133] where neutral ionizable lipids segregate into the hydrophobic core of the LNP bilayer, while the cationic headgroups remain at the membrane-water interfaces. This charge-state dependent segregation of ionizable lipids in the bilayer was also observed in more realistic LNP membranes that include CHOL and PEG-lipids (Figure 3C).[16] More importantly, interactions between PEG oxygen atoms and the charged headgroups of ionizable lipids (at low pH) induce negative curvature due to their attractive interactions, whose extent differs between different ionizable lipids. This is reflected in different exposure of the PEG-lipid linkage among different ionizable lipid types, suggesting that interactions between ionizable cationic lipids and PEG can be optimized for optimal drug delivery.

4.4. Synaptic Vesicle Fusion. The Ca^{2+}-triggered release of neurotransmitters from a synaptic vesicle is key for communication between neurons. At the initial stage, the vesicles are tethered to the plasma membrane through SNARE complex-mediated docking[135] and then undergo priming processes[136] for fast fusion upon Ca^{2+} influx induced by an action potential,[137] which is sensed by synaptotagmin-1 (Syt1).[138] Tightly bound complexin-1 to the SNARE complex promotes the formation of a primed state and inhibits premature fusion.[139,140] Although continuum and CG models provide insight into SNARE-mediated fusion,[141−145] the primed states have not been modeled and simulated until recently. In the simulation of the first all-atom model of a synaptic vesicle in a primed state, it was observed that trans-SNARE complexes bridge the synaptic vesicle and planar bilayer membrane with fragments of Syt1 and/or complexin-1 (Figure 3D).[134] The vesicle was prepared using modified scripts for building CG vesicles from *Martini Maker*. The simulations provide new insight that extensive interactions of the C_2B domain of Syt1 with the planar membrane and a spring-loaded configuration of complexin-1 prevent premature fusion but keep the system ready for fast fusion upon Ca^{2+} influx.

4.5. Methods for Generating Asymmetric Bilayers. Current methods for generating bilayer simulations are based on assumptions appropriate for symmetric bilayers, which include individual area per lipid (APL)-based, leaflet surface area matching (SA)-based, and zero leaflet tension (0-DS)-based methods. Figure 3E shows the APL- and SA-based methods. In asymmetric bilayers, the assumptions may not be applicable, for example, when an asymmetric bilayer has a nonzero spontaneous curvature due to asymmetry in bending moduli and associated spontaneous curvatures of each leaflet. Thus, methods for generating initial conditions for realistic asymmetric membrane simulations remain to be established. In a recent study, another generation method was proposed, which aims to achieve a partial chemical potential equilibrium

https://doi.org/10.1021/acs.jctc.2c01246
J. Chem. Theory Comput. 2023, 19, 2161−2185

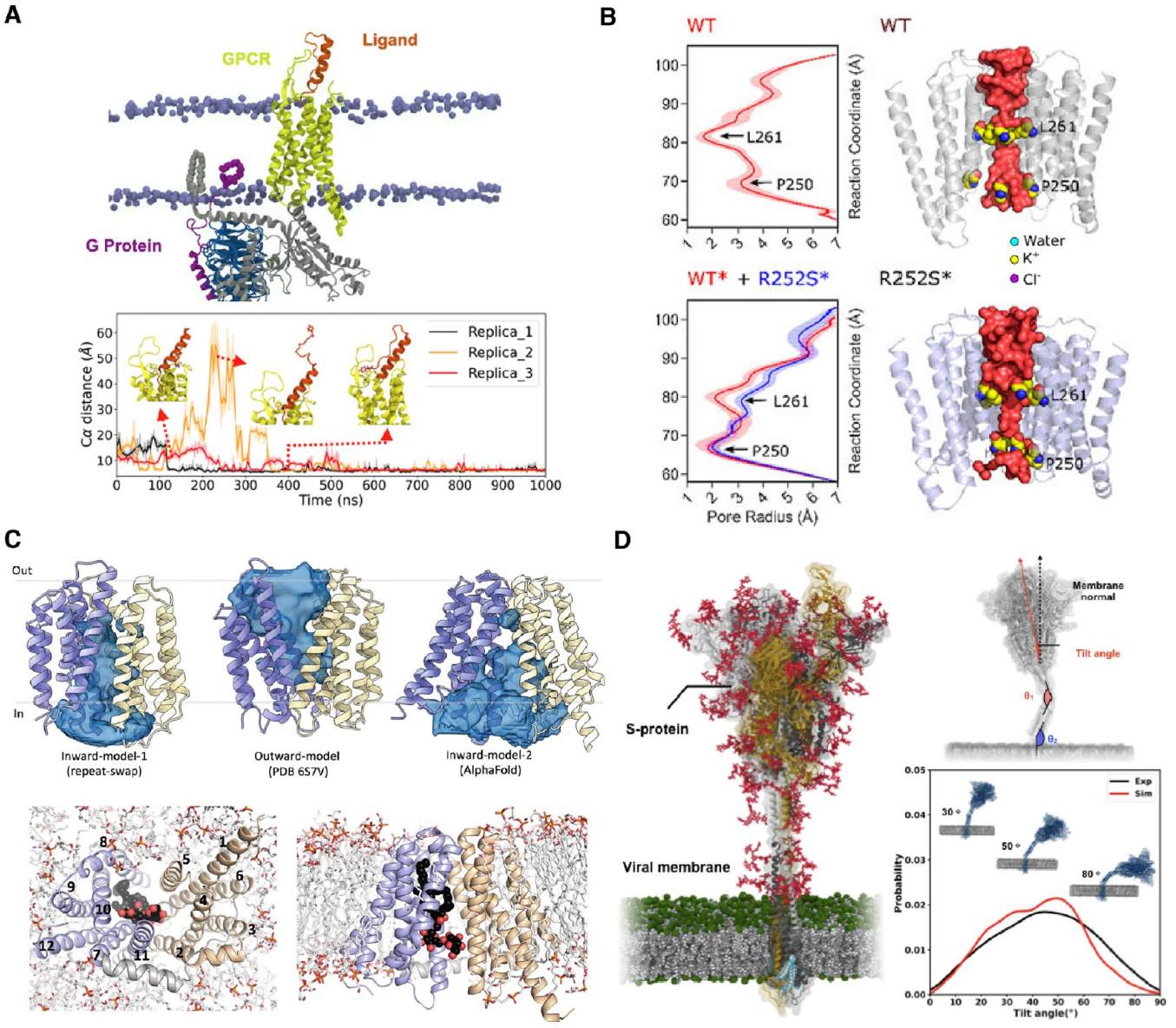

Figure 4. MD simulations to study membrane protein structure, dynamics, and function. (A) Binding of neuropeptide Y onto the GPCR protein Y1 receptor and its tilt angle time series. Adapted with permission from ref 152. Copyright 2022 Chaehee Park et al. Published by Springer Nature. (B) Pore permeation profile of ligand-gated pentameric glycine receptor wild type versus mutant. Adapted with permission from ref 169. Copyright 2022 Mhashal, Yoluk, and Orellana. Published by Oxford University Press. (C) Different states of the LtaA lipid transporter and lateral opening, which leads to lipid substrate diffusion into the pocket. Adapted with permission from ref 170. Copyright 2022 Elisabeth Lambert et al. Published by Springer Nature. (D) Spike protein of SARS-CoV2 and the hinge dynamics of the membrane-anchored complex. Adapted with permission from ref 19. Copyright 2021 American Chemical Society.

between the upper and lower leaflets by interleaflet exchange of selected lipids via $P2_1$ periodic boundary conditions, without altering the bilayer's spontaneous curvature.[39] This approach results in better agreement in mechanical properties between asymmetric bilayers generated by APL-, SA-, and 0-DS-based approaches, in which changes are the smallest for bilayers from the SA-based method. Based on this, the SA/$P2_1$-based or SA-based (when the differential tension is small) approach is recommended as a practical method for generating the initial conditions for asymmetric bilayer simulations.

5. MEMBRANE PROTEIN SIMULATIONS

The Concise Guide to Pharmacology 2021/22, a biennial collection by The British Journal of Pharmacology, summarizes ~1,900 important drug targets and their pharmacology.[31] The collection focuses on six major pharmacological targets including (i) G protein-coupled receptors (GPCRs), (ii) ion channels, (iii) nuclear hormone receptors, (iv) catalytic receptors, (v) enzymes, and vi) transporters. In the following sections, we discuss computational studies on GPCRs, ion channels, and transporters since they are typical membrane proteins and the research of these proteins benefits greatly from CHARMM-GUI *Membrane Builder*. In addition, we devote a subsection on viruses, due to the recent COVID-19 pandemic and an exploding number of publications on virus study.[146,147]

5.1. G Protein-Coupled Receptors. GPCRs mediate cell responses to small molecules, neurotransmitters, and hormones, laying the basis for vision, olfaction, and taste.[148]

https://doi.org/10.1021/acs.jctc.2c01246
J. Chem. Theory Comput. 2023, 19, 2161−2185

GPCRs share a seven α-helical transmembrane (TM) structure template, and in vertebrates, they are categorized into five families: rhodopsin (class A), secretin (class B), glutamate (class C), adhesion, and Frizzled/Taste2.[148] The GPCR's ability to interact with G proteins and secondary messengers and to initiate the downstream signaling pathways makes it multifaceted in functions and important in the central nervous system.[149]

GPCRs play a vital role in relaying information from neurotransmitters and hormone by transmitting the binding of these molecules from the extracellular side to signals on the intracellular side via binding with cellular transducers such as G protein or β-arrestin. MD simulations have been extensively used to study GPCR interactions with signaling molecules[150−155] as well as transducers in the cytosolic side.[156−158] For example, Park et al. recently studied the neuropeptide Y and Y1 receptor,[152] which is enriched in the brain and responsible for neurological processes such as food intake, anxiety, obesity, and cancer.[159,160] The cryo-EM structure shows the binding of neuropeptide Y to Y1 receptor, and MD simulations further reveal the stability and dynamics of the neuropeptide Y binding, providing a conformational ensemble of binding interactions (Figure 4A). Other studies have examined the GPCR-G protein binding and tried to derive a rationale for signaling through different G proteins or β-arrestin.[156−158] Zhao et al. studied β2 adrenaline receptors and their differential binding interfaces with Gs, Gi, and β-arrestin 1.[158] Since the binding interface is different for each cellular transducer, the conformational rearrangement in the TM domain is also different, allowing signal transduction to happen.

The cavities on the extracellular and intracellular sides of the GPCR seven α-helical TM bundle are not only interfaces for signaling peptide and transducer binding but also promising drug-binding sites for modulating receptor activity. In combination with structural biology efforts, MD simulations have been used to study drug binding and analyze the induced conformational changes in GPCRs.[161−164] Of particular interest is distinguishing the agonist and antagonist of GPCRs, as the conventional ligand docking reveals ligands that bind to the pocket but cannot indicate a ligand to be an agonist, an antagonist, or inversed agonist. Studies by Lee et al.[165] and by Shiriaeva et al.[166] examined the boundary between agonist and antagonist on A_3 and A_{2A} adenosine receptors, respectively, and derived the rationale that antagonists restrict the conformational rearrangement required for activation.

The seven α-helical TM bundle also represents a great example for protein allostery. How ligand or protein binding leads to specific conformational change and how the conformational wave is propagated are interesting topics both from a molecular machine perspective and from a pharmaceutical development purpose. Velazhahan et al. studied how the allosteric transition is passed between the dimer interface of Ste2 through MD simulations.[167] Dutta, Selvam, and Shukla examined the allosteric effects on Na^+ ion binding to the CB1 receptor using adaptive sampling on Na^+ ion binding and Markov state models.[168] Therefore, MD simulations greatly extend our understanding of binding of signaling peptide, cellular transducer (G proteins, beta-arrestin), ligands, as well as the allosteric conformational network.

5.2. Ion Channels. Ion channels are the second largest target for available drugs after GPCRs.[171] The arrival of new, fast high-throughput screening platforms and hundreds of ion channel structures makes them increasingly promising targets for therapeutic development.[172,173] Ion channels are classified into three types according to the International Union of Basic and Clinical Pharmacology/British Pharmacological Society (IUPHAR/BPS) classification: ligand-gated ion channels, voltage-gated ion channels, and other ion channels.[174]

Ligand-gated ion channels include 5-HT3 receptors, acid-sensing ion channels, epithelial sodium channel, $GABA_A$ receptors, glycine receptors, ionotropic glutamate receptors, IP3 receptors, nicotinic acetylcholine receptors, P2X receptors, and zinc-activated channels. By convention, these channels are opened or gated by binding of neurotransmitters or endogenous ligands. Voltage-gated ion channels include two-pore channels, cyclic nucleotide-regulated channels (HCN), potassium channels (K_{Ca}, K_{Na}, Kir, K_{2P}, K_V), ryanodine receptors, transient receptor potential (TRP) channels, voltage-gated calcium (Ca_V), proton (H_V1), and sodium (Na_V) channels. In addition, other ion channels include aquaporins, chloride channels (ClC, CFTR, CaCC, VRAC, Maxi Cl), connexins, pannexins, piezo channels, and store-operated ion channels (Orai). The boundary between ligand-gated and voltage-gated ion channels is getting blurry due to the discovery of multimodality ion channels such as TRP channels.[175] The TRP channels can be modulated by various stimuli such as voltage, osmotic pressure, pH, temperature, and natural compounds.[176] This family, alongside with other ion channels, represents an exciting repertoire of targets for biophysical studies and for drug discovery given their roles.[177]

One of the popular topics in ion channels is the permeation of ion and water through their pores.[178−180] MD simulations are commonly employed to study the permeation, providing atomistic insight on top of the typical static pore profile using programs like HOLE2.[181] For example, Mhashal et al. used all-atom simulations to study water permeation in the glycine receptor pentameric ion channel.[169] Taking advantage of statistical physics, MD simulations can also be used to calculate a permeation free energy profile and thus provide a detailed gating mechanism of ion permeation. The derived energy landscape helps to identify important restriction residues and energy barriers.[182−186] Mhashal et al. also studied cancer mutations found in genomic-wide tumor screens.[169] MD simulations show that mutation (R252S) leads to wider upper and lower gates than wild type, facilitating ion and water permeation (Figure 4B). Because of the ion channels' role in the central nervous system and cell metabolism, mutations of ion channels can lead to neurological disease and other diseases such as cancers.[169,187−189] Therefore, there is a huge demand to understand how mutations affect channel conformation and ion permeation. Moreover, in the era of precision medicine, personalized structural biology becomes important to understand variants and mutants.[190] It is impossible to solve structures of every variant, and thus MD simulations that mutate the original protein and study the conformational dynamics become essential.

Another important aspect about the ion channel is drug binding. MD simulations are used to explore ligand binding stability and to better assess the induced-fit effect from docking results[191,192] or to verify the binding poses from structural biology works.[193,194] Ligand-binding free energy calculations yield a quantitative profile for comparison with experimental

https://doi.org/10.1021/acs.jctc.2c01246
J. Chem. Theory Comput. 2023, 19, 2161−2185

measurements.[194] In addition, the dynamical effects exerted by ligands can be accessed from simulation trajectories. Mernea et al. combined terahertz (THz) spectroscopy and MD simulations and showed the binding site of an epithelial sodium channel blocker and reduced channel dynamics upon blocker binding.[195] As more efforts poured into ion channel drug discovery from both experimental and computational approaches, the ligand-binding, modulation, mutations, and permeation pathway of ion channels will be further illuminated.

5.3. Transporters. Transporters translocate chemicals across the membrane, which is vital for cell growth and removing toxic substances. Deficiency in transporters can lead to neurodegenerative diseases[196] and metabolic disorders.[197] Upregulation of ATP-binding cassette (ABC) transporters, such as P-glycoprotein, multidrug resistance-associated protein 2, and breast cancer resistance protein, can efflux drugs in cancer cells and develop multidrug resistance.[198] In Gram-negative bacteria, a number of transporters, such as the Lpt transporter and the Mla transporter, are deployed to maintain the bacterial outer membrane asymmetry.[199,200] Understanding the transporting mechanism and developing drugs to destroy such mechanisms can tackle antibiotic resistance.[201]

Transporters are generally classified into the four major categories: (i) P-type ATPases, which are multimeric and transport primarily inorganic cations; (ii) F-type or V-type ATPases, which are proton-coupled and serve as transporters or motors; (iii) ABC transporters, which are involved in drug disposition and translocating endogenous solutes; and (iv) the SLC superfamily, a gigantic superfamily of solute carriers with 65 families and around 400 members.[202] The SLC superfamily transports a wide variety of solutes, including inorganic ions, amino acids, sugars, and relatively complex organic molecules.[202]

MD simulations can capture substrate movement in transporters. Lambert et al. used MD simulations to study LtaA, a proton-dependent major facilitator superfamily lipid transporter that is essential for lipoteichoic acid synthesis in the pathogen *Staphylococcus aureus*.[170] In their study, both inward-open and outward-open conformations of the transporter were illustrated by examining the solvent accessibility of the cavities (Figure 4C). Notably, the simulations revealed that the lipid substrate (gentiobiosyl-diacylglycerol) permeates into the lower region of the lateral gate through the lateral opening of the translocation channel. This provides evidence for substrate binding and supports for their "trap-and-flip" hypothesis.

As some transporters are driven by proton and/or Na^+ gradients, it becomes important to identify the proton and Na^+ binding sites. Raturi et al. studied the binding and disassociation of Na^+ in a MATE (multidrug and toxic compound extrusion) transporter by simulating the transporter with Na^+ prebound and by letting the Na^+ freely diffuse into the sites.[203] Zhao et al. similarly studied the Na^+ binding in another MATE transporter.[204] Bavnhøj et al., on the other hand, used constant pH simulations to determine the protonation states of sugar transporter protein STP10 and established the basis for proton-to-glucose coupling.[205]

Free energy calculations add further details to transportation pathway studies.[206−209] Prescher et al. studied ABCB4, a human PC lipid floppase, using umbrella sampling along the putative translocation pathways defined by TM1 and TM7 helices, respectively.[207] The free energy profiles show that translocation along TM1 has decreased energy barriers, while the pathway along TM7 does not. The study also compared the translocation based on inward-open versus outward-open states along TM1 and found that the outward-open state is favored for the first part of translocation (binding, positioning, initial translocation) and the inward-open state is favored for the energetically most demanding step (translocating across the bilayer center). The lowered energy barrier value is also close to a previously calculated value from rate difference in experimental measurements. Therefore, MD simulations provide a powerful way to further determine the atomistic details and energetic description about transporter functions.

5.4. Viral Proteins. Common viruses, including HIV, SARS-CoV, Ebola, dengue, Zika, and hepatitis B/C/E viruses, have caused pandemics in human history and brought great suffering to millions of people.[210−213] One prominent example is the recent COVID-19 pandemic. To accelerate drug development against coronavirus, computational tools, such as molecular docking, MD simulations, and free energy calculations, have been widely employed.[147]

Viral infection involves contact with and intrusion into host membranes. Viruses generally have a membrane structure to keep the nucleic acids inside the viral vesicle. Consequently, studies have focused on the membrane proteins that mediate cell binding (such as spike protein gp120) and viral membrane proteins (such as matrix protein and envelope protein E).[214−216] Choi et al. studied the dynamics of the fully glycosylated full-length spike protein of SARS-CoV-2 anchored in a viral lipid bilayer.[19,217] Spike protein is important for host cell entry by binding to ACE2 protein in the host cell membrane. MD simulations reveal the spike protein orientation and dynamics characterized by rigid bodies of different parts (Figure 4D). Full-length glycans were all modeled to reveal the epitopes suitable for antibody binding without being blocked by glycans. In a follow-up study, Cao et al. then examined the binding of the spike protein with six human antibodies, taking glycans into account.[218] Kim et al. used steered MD simulations to examine their binding strength between ACE2 and spike protein from COVID-19 variants.[219,220]

Besides coronavirus, other viruses were also studied in MD simulations. To explore the first step of viral particle fusion with late endosome, Villalaín simulated the dengue virus envelope protein binding to the late endosomal membrane.[214] Jacquemard et al. investigated the interaction between HIV gp120 and CCR5 receptor.[221] Norris et al. studied M matrix protein assembly in measles and Nipah virus infection and showed how the matrix polymerization process was facilitated by PIP_2 lipids.[216] The above research topics showcase the importance of membrane protein studies in viruses and provide a dynamic picture of viral proteins, viral matrix assembly, and cell infection.

6. MEMBRANE-ACTIVE PEPTIDES/PERIPHERAL PROTEINS

6.1. Antimicrobial Peptides. Antimicrobial peptides (AMPs) are naturally occurring peptides in the innate immune systems and have broad-spectrum antimicrobial properties against invading microorganisms.[222] AMPs also have anticancer, antiviral, antiparasitic, and wound-healing properties that make them attractive for pharmaceutical development.[223] The potential mechanisms of membrane disruption by AMPs include the carpet model, barrel-stave model, toroidal pore

https://doi.org/10.1021/acs.jctc.2c01246
J. Chem. Theory Comput. 2023, 19, 2161−2185

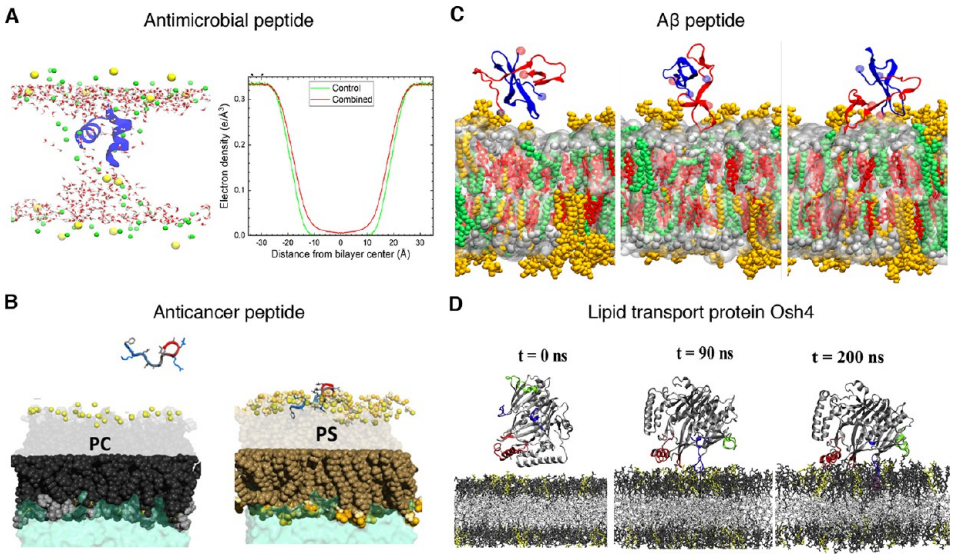

Figure 5. (A) Antimicrobial peptide WLBU2 penetrates into the Gram-positive bacteria membrane and induces water permeation at the membrane center. Adapted with permission from ref 17. Copyright 2022 American Chemical Society. (B) Anticancer peptide HB3 mut3 (with KK motif replaced by RR) penetrates deeply into the PC/PS mixed membrane. Adapted with permission from ref 225. Copyright 2022 Claudia Herrera-León et al. Published by MDPI. (C) Dimerization of Aβ42 and its interactions with the POPC membrane with different binding configurations shown. Adapted with permission from ref 18. Copyright 2021 National Academy of Sciences. (D) Lipid transport protein Osh4 binding to anionic lipid membrane and the interaction sites revealed by HMMM and all-atom MD simulations. Adapted with permission from ref 230. Copyright 2022 Biophysics Society.

model, and aggregate model,[222] which require detailed atomistic examination of AMPs' interactions with membrane bilayers.

The majority of the AMP simulations have explored how AMPs influence the membrane bilayer structure. Allsopp et al. studied AMP WLBU2 in the Gram-negative bacterial inner membrane and Gram-positive bacterial membrane in different binding configurations (straight, bend, and inserted).[17] In the inserted configuration, WLBU2 induces ion and water permeation across the bilayer, indicated by water densities in Figure 5A. In order to see more dramatic membrane disruption phenomena at a much longer time scale, CG simulations are usually necessary. Miyazaki and Shinoda studied the action of melittin on membranes with a varying peptide-to-lipid (P/L) ratio.[224] At a P/L ratio = 1/50, toroidal pore formation was observed, while at a P/L ratio = 1/26, lipid extraction by melittin accompanying pore formation was observed. This highlights the influence of AMP concentrations on its mechanistic action modes and add a further holistic picture to all-atom simulations.

Other MD simulation studies on AMPs aim to understand their selectivity and targeting. MD simulations on anticancer peptides have shown that they preferentially bind to cancer cells due to the exposed PS lipids on the cell surface (Figure 5B).[225] Meanwhile, CHOL has been shown to lower the penetration of AMPs into the membrane, partially due to the more ordered membrane environment.[226] This lays the foundation for AMPs' targeting to microbial membranes rather than being toxic to mammalian cells. Lantibiotics, a type of modified peptides, are promising candidates to fight against resistant bacterial strains.[227] MD simulations show that they preferentially bind to lipid II, the precursor in the peptidoglycan biosynthetic pathway, and induce a water tunnel in the membrane.[228]

Overall, the research landscape of AMPs requires (i) structural characterizations of the usually short peptide, which does not have an experimental structure, so MD simulations can be used to validate the predicted structure and study the structural change under different environmental conditions including pH;[229] (ii) an atomistic or near-atomistic picture of peptide-membrane interactions, and (iii) rationales about peptide targeting and cell selectivity based on cell membrane compositions. All of the above can be studied through *Membrane Builder* and *Martini Maker* in CHARMM-GUI.

6.2. Aβ and Protein Aggregates. Mammalian amyloids are highly ordered fibrous cross-β protein aggregates that are implicated in a variety of diseases, including Alzheimer's disease, Parkinson's disease, type 2 diabetes, and prion diseases.[231] The Aβ peptide aggregates on the neuronal membrane are linked to Alzheimer's disease. Fatafta et al. studied Aβ42 dimer in solution and in the presence of a lipid bilayer using MD simulations.[18] The results show that Aβ42 peptides attached to the membrane and interacted preferentially with ganglioside GM1 (Figure 5C). Experimentally, Zhang et al. later showed that GM1 promotes early Aβ42 oligomer formation in liposomes and helps to maintain the amyloid structure.[232] The authors then mutated the Arg residue responsible for GM1 binding in MD simulations and found much more disassociation of Aβ42 from the membrane.

Apart from the Aβ peptide, α-synuclein (αS) is a synaptic peptide that tends to form aggregates in Parkinson's disease. Garten el al. studied αS interactions with different membranes and found that branched lipids (DPhPC) promote membrane absorption through shallow lipid-packing defects.[233] Human Langerhans islets amyloid polypeptide (hIAPP) is the main amyloid found in patients with type 2 diabetes. Espinosa et al. studied the mechanism underlying promoted hIAPP aggregation in a hydroperoxidized (R-OOH) bilayer.[234] The MD simulation results show that the oxidized lipid bilayer increases the helicity of hIAPP and the amyloidogenic core, accelerating the aggregate formation. Protein aggregates, such as Aβ, αS,

https://doi.org/10.1021/acs.jctc.2c01246
J. Chem. Theory Comput. 2023, 19, 2161−2185

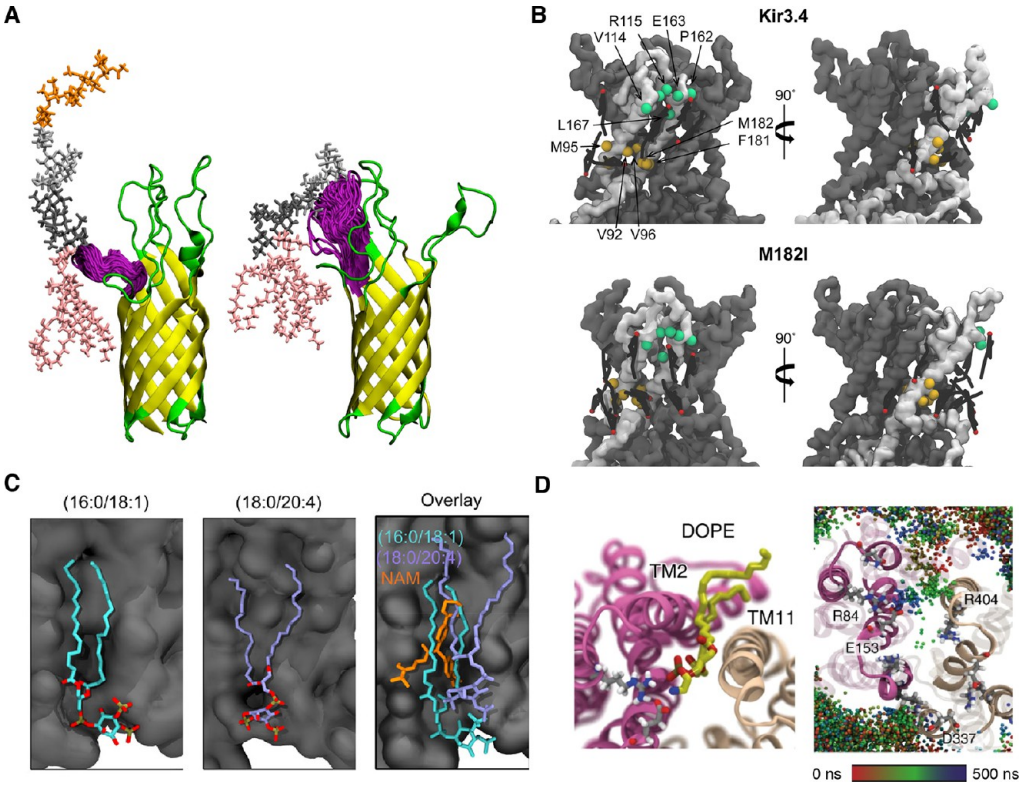

Figure 6. Protein−lipid interactions revealed by MD simulations. (A) Interactions between LPS and outer membrane protein OprH, LPS sugars bind to the flexible hinge in OprH. Adapted with permission from ref 14. Copyright 2016 Biophysics Society. (B) Molecular switch of CHOL binding hotspots in Kir3.4 and its mutation leading to loss of the CHOL upregulation effect. Adapted with permission from ref 250. Copyright 2022 National Academy of Sciences. (C) PIP_2 binding in the glucagon receptor, a class B GPCR protein, and the conformation preference of PIP_2 binding to the inactive state. Adapted with permission from ref 253. Copyright 2022 American Chemical Society. (D) PE lipids disturb the conservative network in XylE transporter and favors the inward-open state. Adapted with permission from ref 254. Copyright 2018 Chloe Martens et al. Published by Springer Nature.

and hIAPP, have significance in disease cure and pharmaceutical development. Studying their interaction with membrane, as well as how drugs disrupt the aggregate-membrane interactions, will pave the way for drug discovery.[235]

6.3. Peripheral Membrane Proteins. Peripheral membrane proteins are a class of membrane proteins that attach to the lipid bilayer, in contrast to integral membrane proteins.[236] Compared with enriched structural biology data about transmembrane proteins like GPCRs and ion channels, peripheral membrane proteins have not been extensively studied, possibly due to the complexity of the protein−membrane interface.[237] The aforementioned protein aggregates like Aβ and αS are also part of the peripheral membrane protein class. In this subsection, we focus on slightly larger peripheral membrane proteins that interact with membranes through electrostatic/hydrophobic interactions, hydrophobic tails, or GPI-anchors.

Osh4 is an oxysterol binding protein in yeast, and its physiological roles include sterol homeostasis and signal transduction.[238] Osh4 is shown to transport sterol between liposomes, and the efficiency is enhanced by anionic lipids (e.g., PS and PIPs) at the target membrane.[239] Karmakar and Klauda studied Osh4 binding to a membrane bilayer using all-atom MD simulations and HMMM models.[230] Since the interaction between Osh4 and the membrane is mostly on the membrane surface, HMMM is a convenient and efficient model for characterizing such interactions. The authors found that both all-atom and HMMM membranes can successfully capture such interactions (Figure 5D). The binding of one facet of Osh4 to the membrane is more favorable than the other two. The simulations also showed the penetration of a phenylalanine loop into the membrane and identified the key interacting residues, in agreement with earlier cross-linking data. Another study by Aleshin et al. combined MD simulations with NMR and X-ray crystallography to study the binding of the pleckstrin homology (PH) domain with PIP lipids. NMR measurements identified key residues involved in PIP binding based on chemical-shift perturbations, while MD simulations further illustrated the binding interface and lipid configurations.[240]

K-ras is a GTPase cycled from a GDP bound "off" state to a GTP bound "on" state, which regulates cell growth.[241] When the gene is mutated, the K-ras protein is constitutively switched on, allowing cells to grow uncontrollably and activating downstream pathways. K-ras mutations are found in about 30% of all human tumors and are the frequent drivers for pancreatic, colorectal, and lung tumor cases.[241] Lu and Martí simulated G12D mutant of KRas-4B, a mutant common in cancers, and found two main orientations relative to the membrane.[242] They further used well-tempered metadynamics simulations to derive the free energy of the binding configurations. The authors also found that GTP-binding to KRas-4B influences protein stabilization and can help open the Switch I/II druggable pockets. Given the difficulties in resolving the atomistic details of peripheral membrane protein binding to membranes, MD simulations offer a unique

https://doi.org/10.1021/acs.jctc.2c01246
J. Chem. Theory Comput. 2023, 19, 2161−2185

opportunity to identify important binding configurations and lay the basis for interpreting biophysical measurements such as cross-linking, NMR, and FRET.[240]

7. PROTEIN−LIPID INTERACTIONS

7.1. LPS-Outer Membrane Protein in Gram-Negative Bacteria. Gram-negative bacteria possess two lipid bilayers: an inner and an outer membrane. The inner membrane is composed of phospholipids, while the outer membrane consists of phospholipids in the inner leaflet and LPS in the outer leaflet.[243] The stability and impermeability of the outer membrane highly contribute to the antibiotic resistance of some pathogenic Gram-negative bacteria such as *Pseudomonas aeruginosa*.[244] LPS lipids are composed of three regions: lipid A, a hydrophilic core oligosaccharide attached to lipid A, and an O-antigen polysaccharide with a varying length of up to ∼25 repeating units.

Lee et al. investigated the interaction between outer membrane protein OprH and LPS by simulating OprH protein in three membranes with (i) lipid A, (ii) lipid A + core, and (iii) lipid A + core + O10-antigen in the outer leaflet.[14] Their simulations show that the membrane thickness decreases around the protein due to the interactions between protein residues and LPS lipids. The extracellular loops of OrpH are highly charged and interact with both lipid A and O10-antigen through hydrogen bonds. In terms of dynamics, loop 2 is less dynamical in the longer full LPS membrane than in the shorter LPS membrane (Figure 6A). Such protein-LPS interactions explain why OprH can act as a membrane stabilizer and function to cross-link LPS when the divalent ion concentration is low.[245] LPS represents a complex lipid structure, and its role in Gram-negative bacteria is important for bacterial drug resistance. Therefore, understanding the protein−lipid interactions in such membranes is of significance.

7.2. Search of Cholesterol Binding Motifs. CHOL is a vital component of mammalian plasma membranes and increasingly found to impact functions of a growing number of ion channels[246] and GPCRs.[247] Common motifs such as CRAC (cholesterol recognition/interaction amino acid consensus), CARC (the reverse sequence of CRAC), or CCM (cholesterol consensus motif) are putative CHOL-binding motifs.[248,249] Studies, however, found that CHOL can also bind to other structural elements tightly.

Corradi et al. used CG simulations to study CHOL binding in Kir3.4, a potassium ion channel upregulated by CHOL.[250] The authors identified a Met residue that, once mutated into Ile, made the effect of CHOL turn into downregulation. Through the long-time scale simulations of Kir3.4 wild type and M182I mutant in the CHOL-containing membranes, the CHOL binding hot spots were identified on the protein surface. The binding difference between the wild type and mutant shows that, in the mutant, the CHOL binding at the inner leaflet region is dominant and mostly located at the interface of neighboring subunits (Figure 6B). The study hypothesizes that the distribution of CHOL on protein surface plays a critical role in switching the regulation direction of CHOL.

Accompanying the development of PyLipID, a tool for analyzing protein−lipid interactions in MD simulation trajectories, Song et al. performed large-scale simulations for 10 class A and B GPCRs.[251] They identified on average 14−17 CHOL binding sites per receptor. They then studied a total of 153 CHOL binding sites and classified the sites into strong vs nonspecific binding sites based on the buried area and CHOL residential time. Strong cholesterol binding sites have increased occurrence of Leu, Ala, and Gly residues, though these sites lack specific CHOL-binding motifs, which is also found in another study showing that there is no broadly recurring CHOL-binding motifs in GPCRs.[252] The CHOL molecule is hydrophobic with the hydroxyl group providing potential hydrogen binding and polar interactions. Therefore, the binding of CHOL is mostly driven by hydrophobic interactions with protein, which partially leads to a lack of universal CHOL-binding motifs.[194] This further requires more case-by-case studies on individual membrane proteins to identify their CHOL binding sites.

7.3. Phosphatidylinositol Phosphate (PIP) Binding. Phosphoinositides (PIPs), phosphorylated derivatives of phosphatidylinositol (PI), are essential components of eukaryotic cell membranes. PIPs play important roles in cell membrane dynamics, focal adhesion, action organization, and intracellular signaling[255] and serve as modulators of GPCRs,[253] ion channels,[256] and transporters.[257] The hydroxyl groups on the inositol ring of PI can be phosphorylated at the 3, 4, and 5 positions by specific kinases, giving rise to a group of structurally related PIPs, such as PI-monophosphate (PI3P, PI4P, and PI5P), PI-*bis*phosphate ($PI(3,4)P_2$, $PI(3,5)P_2$, and $PI(4,5)P_2$), and PI-*tris*phosphate ($PI(3,4,5)P_3$).[258]

To elucidate PIP_2 binding on the glucagon receptor, a class B GPCR protein, Kjølbye et al. used MD simulations to examine the binding of three types of $PI(4,5)P_2$ lipids with varying tails to the receptor.[253] The simulations show that the three PIP_2 lipids have different binding profiles on the receptor. Notably, both (16:0/18:1) PIP_2 and (18:0/20:4) PIP_2 bind to the site between TM6/7 and H8 (Figure 6C). This site was also previously found to be the binding site of a negative allosteric modulator. Examining the conserved network and key indicators of active vs inactive forms shows that PIP_2 lipids induce more inactive states than active states.

PIP lipids are also indispensable for ion channel regulations.[259−261] Feng et al. recently studied PIP lipid binding to the TRPV2 ion channel and identified a region near the membrane-proximal area that binds to PIP lipids tightly.[194] Through μs-long simulations, the PIP lipids gradually diffuse into the region and remain bound. This same region was previously found to be the putative PIP binding site by in vitro experiments.[262] The simulation results provide a 3D structural context of the PIP binding site formed by S1, S2, and C-terminal membrane proximal regions.

Especially for integral membrane proteins, the binding sites of PIP lipids are usually difficult to predict in experiments. Cryo-EM structures are becoming more prevalent for understanding protein−lipid interactions, but due to the resolution and the mobility of lipids, it is hard to solve the PIP binding on membrane proteins. Therefore, MD simulation becomes a key tool to decipher the PIP binding sites as well as their dynamics.

7.4. Phospholipid Wedged in Proteins. Besides the aforementioned CHOL and PIP lipids, other phospholipids such as PC, PE, PG, and cardiolipin also interact with membrane proteins and modulate the protein conformations. Martens et al. studied xylose transporter XylE, consisting of both N- and C-lobes.[254] During MD simulations, PE lipid diffused into the N- and C-lobe interface and disrupted the charge relay network formed by Glu or Asp (Figure 6D). PC lipids were not observed to have the same behavior, possibly

https://doi.org/10.1021/acs.jctc.2c01246
J. Chem. Theory Comput. 2023, 19, 2161−2185

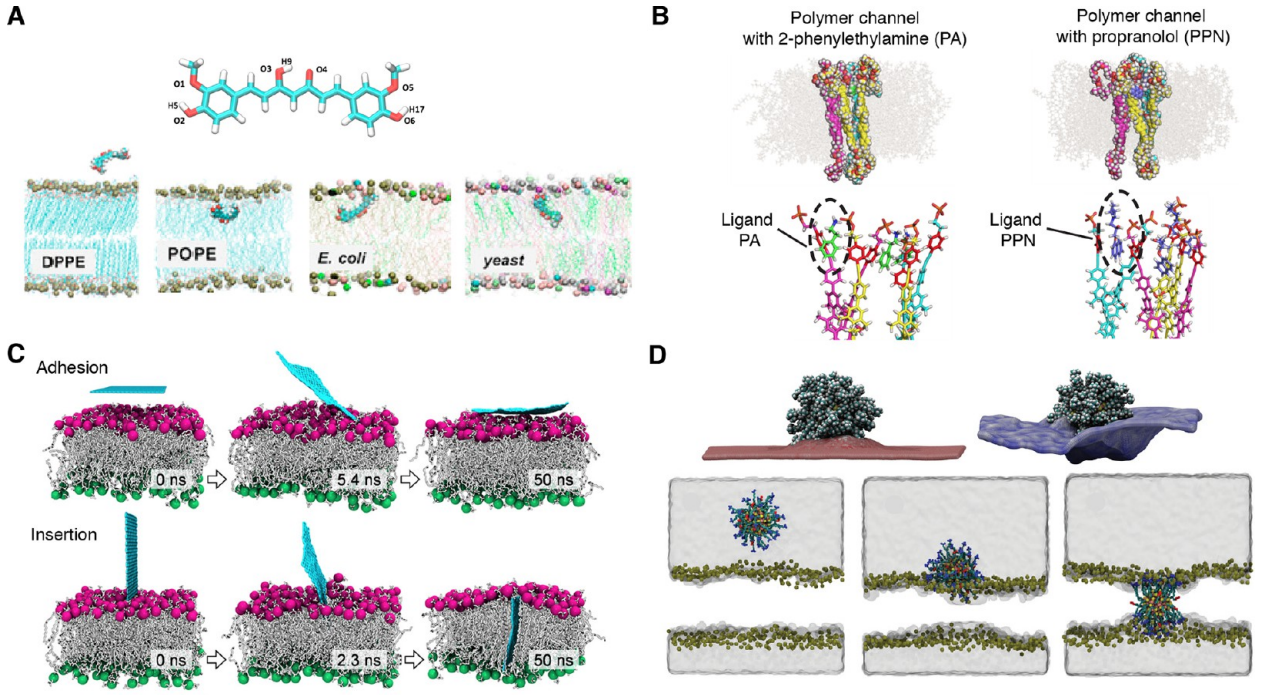

Figure 7. Drug-membrane interactions and nano-biomembrane interfaces revealed by MD simulations. (A) Curcumin, a natural compound from turmeric and its interactions with different membranes. Adapted with permission from ref 271. Copyright 2018 American Chemical Society. (B) A synthetic multipass transmembrane channel formed by multiblock amphiphiles is ligand-gated by 2-phenylethlamine (PA) or propranolol (PPN). Adapted with permission from ref 284. Copyright 2020 Takahiro Muraoka et al. Published by Springer Nature. (C) Graphene sheet adhesion and insertion to a membrane. Adapted with permission from ref 286. Copyright 2020 American Chemical Society. (D) A gold nanoparticle and its interaction with a lipid membrane. Adapted with permission from ref 287. Copyright 2019 Fabio Lolicato et al. Published by WILEY-VCH Verlag GmbH & Co. KGaA, Weinheim.

due to its larger headgroup than PE. Furthermore, the PE binding in the interface favors the inward-open conformation, consistent with hydrogen−deuterium exchange mass spectrometry observations. This demonstrates the conformational modulation by zwitterionic lipids. Another study by Choi et al. on glutamate transporter GLUT3 found that PE lipids boosted domain−domain assembly of the protein, though anionic lipids failed to have the same effects, demonstrating the role of PE lipids to ease the membrane remodeling during the protein folding.[263]

In other cases, the anionic lipids have a stronger effect due to stronger electrostatic interactions. Neale et al. studied the β2 adrenergic receptor using MD simulations to detect lipid binding in the receptor,[264] because agonist binding is not sufficient to fully stabilize active states.[265] Through simulations, the authors found a PC lipid binding to the crevice between TM6 and TM7, breaking an ionic lock, and stabilizing the active state. Furthermore, they simulated the receptor in a PG-containing membrane and found that anionic PG has a stronger and more stable binding in the same crevice than PC.

Cardiolipin (CL) is a phospholipid with four tails and comprises about 20% of the inner mitochondria membrane phospholipids mass.[266] Yi et al. studied the effects of CL on mitochondrial ADP/ATP carrier protein using MD simulations.[267] By embedding the carrier protein in membranes with and without CL, the authors found that negatively charged CL lipids stabilize the domain 1−2 interaction through binding with surrounding positively charged residues and fold the M2 loop into a defined conformation. These results show how phospholipids can fit into the crevice and serve as molecular wedges in the protein assembly, stabilizing the structure or affecting the assembling process.

8. DRUG-MEMBRANE INTERACTIONS

8.1. Drug Mechanism and Permeation. As drug discovery studies boom, the need for understanding how drugs interact with the membrane becomes more prominent. The drug partition in the membrane can partially contribute to the drug efficacy, while drug location and influence on the membrane properties can dictate part of the toxicity.[268] Natural products and their structural analogs have long been used in pharmacotherapy. In recent years, the improved analytical tools, genomic data mining and engineering strategies, and microbial culturing advances allow more screening, isolation, and characterization of natural compounds.[269] Curcumin, a natural phenolic compound from turmeric, is widely used for food coloring and seasoning, which is antimicrobial, antioxidant, anticancer, and anti-inflammatory.[270] Using MD simulations, Lyu et al. studied curcumin and examined its partition into pure bilayers such as POPE, POPG, POPC, DOPC, DPPE, and mixed membranes including POPE/POPG, *E. coli* membrane, and yeast membrane (Figure 7A).[271] Curcumin is found to stay in the lipid tail region close to the glycerol, mostly with a parallel orientation and a membrane-thinning effect.

A plethora of publications has examined the membrane interactions with a variety of compounds, including psilocin (active hallucinogen of magic mushrooms),[272] ionic liquids,[273,274] cancer drugs,[275] DNA transfection reagent,[15] and dye probes.[276−278] Ionic liquids are liquid salts consisting of organic cations and inorganic anions and are considered a

https://doi.org/10.1021/acs.jctc.2c01246
J. Chem. Theory Comput. 2023, 19, 2161−2185

green alternative to organic solvents.[279] Shobhna, Kumari, and Kashyap found that ionic liquids increase membrane condensing using simulations.[274] Siani et al. studied doxorubicin, a widely used cancer treatment drug, in sphingomyelin-based membranes in order to optimize the liposome-based drug delivery for doxorubicin.[275] Kneiszl, Hossain, and Larsson studied how intestinal permeation enhancers interact with membranes to lay the basis for improving the efficacy of oral administration drugs.[280] Sabin et al. studied polyethylenimine and its interactions with membranes using simulations and showed that polyethylenimine induces pore-forming in the membrane, contributing to an understanding of the DNA cell transfection process.[15] Winslow and Robinson developed a new phase-sensitive membrane raft probe through QM/MM simulations of different probes in the membrane.[276]

The studies of chemical-membrane interactions using MD simulations enable an atomistic understanding of the interactions, allowing calculations of influenced membrane properties and offering molecular details for processes ranging from gene transfection to materials design (ionic liquids, dye probe) and to drug acting mechanisms.

8.2. Artificial Channels. Artificial channels are polymer molecular machines consisting of peptides and polymers in the membrane bilayer, which is designed to mimic structural and functional features of their biological counterparts such as aquaporins, ion channels, and transporters.[281] Functionally, these channels mimic the integral membrane proteins, but chemically, they are synthetic and represent a closer kin to the nanoparticles.

Song et al. designed an artificial water channel based on a cluster-forming organic nanoarchitecture, peptide-appended hybrid[4]arene.[281] Once oligomerized, the channel has a central pore where water and ion can pass through. They used MD simulations to study the water permeation across the 22-mer cluster of the channel and the biological aquaporin-1 and found longer permeation time and path in the artificial channel.

The water permeation is also studied in other artificial water channels made of carbon nanotube[282] or aggregated polymers[283] using MD simulations. For example, Muraoka et al. designed a synthetic ion channel with multiblock amphiphiles and the ion permeation is gated by amine ligands (Figure 7B).[284] When the ligand is bound, the channel is activated; otherwise the channel is deactivated. MD simulations were used to model the assembly and ligand binding to the polymer ion channel. Miao, Shao, and Cai used MD simulations to study an ion transporter consisting of a single molecule spanning the lipid bilayer.[285] MD simulations show that the artificial transporter translocates K^+ ions through alternating U-shape and linear shapes. The free energy of the transporter conformation in the membrane was then calculated using MD simulations. As the structures of artificial channels in the membrane are usually unknown, MD simulations provide a powerful tool to characterize the conformations and functions of the synthetic molecular machines in the membrane.

9. NANO-BIO INTERFACES

Nanomaterials are materials having at least one dimension less than 100 nm.[288] Due to the desired physicochemical and electrical properties often displayed in nanomaterials, they are widely deployed in electronics, biomedicine, and aerospace engineering.[289] The biomedical applications of nanomaterials include drug delivery, diagnostic, and therapeutic agents.[290] As humans are constantly exposed to nanomaterials in the modern society, the nanomaterials find their way into the human body and can induce cell toxicity, immunotoxicity, and genotoxicity.[288,290] Therefore, it becomes imperative to gain insight into the effect of nanomaterials on biomembranes and proteins.

Two-dimensional nanomaterials have a high surface-to-volume ratio, excellent functionalization capabilities, mechanical properties, and inherent optical properties to serve as biosensors, cell culture platforms, and diagnostic imaging reagent.[291] Graphene is one of the most well-known 2D nanomaterials.[292] Zhu et al. studied graphene nanosheets (GNs) and their membrane perturbation effects using MD simulations (Figure 7C).[286] Two types of GN-membrane interactions were studied, adhered vs inserted. The adhered GNs on the membrane surface induce membrane thinning and more flexible lipid conformations, making it more difficult for lipid flipflop due to strong interactions between GNs and lipid head groups. Meanwhile, the inserted GNs lead to the ordering of nearby lipids and generate a nanodomain. Lipid flipflops have a lower barrier when far away from the inserted GNs but a much higher barrier in the vicinity of inserted GNs.

Nanoparticles are nanomaterials that have all three dimensions less than 100 nm.[293] With the recent advances in nanoscience and nanotechnology, there has been an increasing interest in understanding the molecular mechanisms governing nanoparticle−membrane interactions for drug delivery, biomedical applications, and toxicity to human cells.[294] Lolicato et al. reported the role of temperature and lipid charge on cellular intake of the cationic gold nanoparticles (AuNPs) (Figure 7D).[287] By combining neutron reflectometry experiments with all-atom and CG MD simulations, they quantitatively revealed that both the lipid charge and temperature play pivotal roles in AuNP intake into lipid membranes. Foreman-Ortiz et al. integrated experimental and computational approaches to resolve the effect of nanoparticles on the function of membrane-embedded ion channels.[295] They revealed that anionic AuNPs reduce activities of gramicidin A ion channels and extend channel lifetimes without disrupting membrane integrity, in a manner consistent with changes in membrane mechanical properties.

As nanomaterials applications further expand and mature, the toxicity on biological systems can be studied in more atomistic details through MD simulations. CHARMM-GUI *Polymer Builder* and *Nanomaterial Builder* offer polymers such as polyacrylamides, polydienes, polyamines, vinyls, polyesters, and nanomaterials such as carbon nanotube, graphene, graphite, silica, mica, metals, and metal oxides.[40,41] These tools combined with *Membrane Builder* can help design better drug delivery systems for vaccines and biosafe/biocompatible materials.

10. CAVEATS AND PITFALLS IN USING MEMBRANE BUILDER

As illustrated in Sections 4-9, *Membrane Builder* has been applied to numerous research topics for generating initial conditions. Although *Membrane Builder* has greatly facilitated the preparation of initial membrane simulation systems and successfully resolved many issues, such as mutations, modifications, and CHOL and peptide ring penetration by lipids, it is imperative to exercise caution when generating and simulating membrane systems to avoid introducing artifacts that could compromise the simulation results. Here, we list a

https://doi.org/10.1021/acs.jctc.2c01246
J. Chem. Theory Comput. 2023, 19, 2161−2185

few common issues that are not addressed by *Membrane Builder* and for which researchers should be careful in their practical applications.

10.1. System Size. When generating initial conditions, it is crucial to choose an appropriate membrane system size depending on the application type. Based on our own research experiences, we suggest to have at least 2−3 lipid shells between the transmembrane domain and the box edge on the membrane plane (i.e., the *XY*). One should check "step3_packing.pdb" to judge if the membrane size is big enough for their own application. Also, to avoid the artifacts due to the periodic boundary conditions, it is necessary to have enough box size for large extracellular and intracellular domains (e.g., Figures 4A and 4D). In addition, for simulations of spontaneously phase separated membranes, the system size should be sufficiently large to include at least thousands of lipids.[296]

10.2. Initial Lipid Packing. It is essential to inspect the initial lipid packing for any empty space between membrane peptides that could result in unrealistic aggregation. A recent simulation study reveals that the influenza virial fusion peptides in a leaflet aggregate within microseconds time scale.[297] However, when the initial condition lacks sufficient lipids between fusion peptides, it results in unrealistically fast aggregation. In addition, for asymmetric membranes, the surface areas of both leaflets should be carefully matched to avoid large differential tension and altered mechanical properties, which can be significantly reduced by generating initial conditions using surface areas from cognate symmetric bilayers and/or using a $P2_1$-based approach[39] (Figure 3E and subsection 4.5 **Methods for Generating Asymmetric Bilayers**).

10.3. Proper Equilibration. Proper equilibration of any simulation is a crucial aspect that requires close monitoring. While the system sizes usually stabilize in submicrosecond time scales, multicomponent membranes and those with coexisting domains often require simulations of microseconds for equilibrated lipid distributions (around a peptide/protein) and substructures in the Lo phase.[114−116,298] Hence, one should check proper equilibration during the simulation progress, especially for realistic complex membrane simulations.

11. FUTURE DEVELOPMENTS AND APPLICATIONS OF *MEMBRANE BUILDER*

CHARMM-GUI *Membrane Builder* is a user-friendly web tool for various membrane-related simulations. It supports over 670 lipid/surfactant types and provides inputs for most of the common MD engines with various FFs ranging from atomistic models to CG and polarizable models. Different membrane structures including planar bilayers, micelles, vesicles, and nanodiscs can be generated. The linking with other CHARMM-GUI modules allows for building complex systems with protein, nucleic acids, ligands (*Ligand Reader& Modeler*), glycans (*Glycan Reader & Modeler*), glycolipids (*Glycolipid Modeler*), LPS (*LPS Modeler*), polymers (*Polymer Builder*), and nanomaterials (*Nanomaterial Modeler*) and can be combined with enhanced sampling techniques (*Enhanced Sampler*), high-throughput protein−ligand simulations (*High-Throughput Simulator*), and binding free energy calculations (*Free Energy Calculator*). Beside these capabilities, *Membrane Builder* can also be improved and further developed in the following areas.

Lipids are oxidized by enzymes like cyclooxygenases or nonenzymatically by uncontrolled oxidation.[299] The oxidized lipids serve as key signaling mediators and hormones regulating metabolism, cell death, and inflammation, while uncontrolled oxidization can be harmful.[300,301] The oxidized lipid library is currently under development. The library will contain lipids with the PC or PE headgroup and an oxidized *sn*-1 chain including aldehyde, ketone, hydroxyl, peroxide, and carboxyl groups. This will prompt more research on oxidized lipids and their roles in membranes and related proteins.

Mycobacteria such as *Mycobacterium tuberculosis* (Mtb), *M. leprae*, and *M. avium* have a significant impact on human health.[302] Mycobacterial membranes are famous for their complexity uncommon in the Gram-positive bacteria. Mycobacteria have unusually long-chain fatty acids, mycolic acids, which can adopt different folded conformations to form a barrier.[303] Other unique components include trehalose molecules, large branched structures (lipomannan and lipoarabinomannan) spanning the space between the inner and outer membranes, and phthiocerol dimycocerosates (PDIM), the major lipid virulence factors. All of these molecules are currently being implemented into *Membrane Builder,* which could greatly benefit mycobacterial membrane research.

Bicelles are synthetic lipidic discoidal aggregates of the lipid bilayer stabilized by detergents or short-tailed lipids on the rim.[304] Bicelles can be oriented parallelly or perpendicularly to magnetic fields and can be doped with charged lipids, surfactants, or cholesterol to offer a wide variety of membrane environments for structural biology. *Bicelle Builder* is under development to support generating bicelle structures with varying *q* values (lipid to detergent ratios). In addition, all-atom lipid vesicle generation is not available, although it could be built in *Martini Maker* and then converted to all-atom models, which leads to limited types of lipids. *Vesicle Builder* in the future will allow generating vesicles with more diverse all-atom lipid types.

For more complex systems, it is currently difficult to include multiple copies of different components (other than lipids and ions) at desired locations in a membrane or bulk. Also, generating multilamellar membranes is not supported, which can be useful for establishing asymmetric environment on each side of the bilayer. For studying interactions between nanoparticle and biological membranes and between peptide and membrane-like polymers,[286,287,295,305] systematic generation of such systems is not available in CHARMM-GUI yet. The above issues will be addressed by *Multicomponent Assembler* in CHARMM-GUI in the near future, which will allow easy generation of realistic biological membranes and nano-bio interfaces.

MD simulation is restricted by the existing bonded structure in the FF, while there are millions of reactions happening in the biological systems that involve bond breaking and forming. Quantum mechanics/molecular mechanics (QM/MM) methods are a well-established approach to overcome this limitation of MD simulation and study enzymatic reactions.[306] The description of the reactive part of enzyme takes place through QM, while the remaining majority of biomolecules is treated by MM. *QM/MM Interfacer* in CHARMM-GUI is recently released and will benefit research on drug binding and enzymatic reactions in membrane proteins.

From the applications in the CHARMM-GUI community, we note that the membrane simulations are increasingly serving as a computational microscopy with statistical reliability.[12] Processes occurring in or out of the membrane surface, including vesicle fusion, DNA transfection, virus

https://doi.org/10.1021/acs.jctc.2c01246
J. Chem. Theory Comput. 2023, 19, 2161−2185

infection, substrate translocation, nanopore sequencing, drug delivery, protein detergent extraction, and pollutant toxicity, as well as mutation and drug-induced protein conformational changes, can all be visualized and analyzed at the atomistic level.[15,16,19,86,134,169,170,194,221,307,308]

We expect membrane and membrane protein simulations in the next decade to further explore all kinds of aforementioned processes, revealing disease mechanisms, facilitating biosafe material design, and improving drug efficacy. Meanwhile, we hope that *Membrane Builder* continues to serve the broad scientific community as an integration platform to prepare and execute various general and advanced simulations, with many packages and methods on the platform developed by researchers across the simulation communities.

AUTHOR INFORMATION

Corresponding Author

Wonpil Im − *Departments of Biological Sciences and Chemistry, Lehigh University, Bethlehem, Pennsylvania 18015, United States;* orcid.org/0000-0001-5642-6041; Email: wonpil@lehigh.edu

Authors

Shasha Feng − *Departments of Biological Sciences and Chemistry, Lehigh University, Bethlehem, Pennsylvania 18015, United States;* orcid.org/0000-0003-3394-6911

Soohyung Park − *Departments of Biological Sciences and Chemistry, Lehigh University, Bethlehem, Pennsylvania 18015, United States;* orcid.org/0000-0002-4883-3031

Yeol Kyo Choi − *Departments of Biological Sciences and Chemistry, Lehigh University, Bethlehem, Pennsylvania 18015, United States;* orcid.org/0000-0002-4218-7139

Complete contact information is available at: https://pubs.acs.org/10.1021/acs.jctc.2c01246

Author Contributions

S.F., S.P., and Y.K.C. contributed equally to this work.

Notes

The authors declare the following competing financial interest(s): W.I. is the co-founder and CEO of MolCube, Inc.

ACKNOWLEDGMENTS

The authors thank Emanuel Luna, Lingyang Kong, Yiwei Cao, Donghyuk Suh, Hugo Guterres, and Nathan Kern for proofreading and critiques on this manuscript. This work was supported in part by the grants from US National Institutes of Health GM138472 and National Science Foundation OAC-1931343, DBI-2011234, and MCB-2111728.

REFERENCES

(1) Alberts, B.; Johnson, A.; Lewis, J.; Raff, M.; Roberts, K.; Walter, P. Chapter 10. Membrane Structure. In *Molecular Biology of the Cell*, 4th ed.; Garland Science: New York, 2002.

(2) Berkowitz, M. L.; Raghavan, K. Computer simulation of a water/membrane interface. *Langmuir* **1991**, *7* (6), 1042−1044.

(3) Wendoloski, J. J.; Kimatian, S. J.; Schutt, C. E.; Salemme, F. R. Molecular Dynamics Simulation of a Phospholipid Micelle. *Science* **1989**, *243* (4891), 636−638.

(4) Edholm, O.; Berger, O.; Jähnig, F. Structure and Fluctuations of Bacteriorhodopsin in the Purple Membrane: A Molecular Dynamics Study. *J. Mol. Biol.* **1995**, *250* (1), 94−111.

(5) Woolf, T. B.; Roux, B. Molecular dynamics simulation of the gramicidin channel in a phospholipid bilayer. *Proc. Natl. Acad. Sci. U. S. A.* **1994**, *91* (24), 11631−11635.

(6) Pastor, R. W. Molecular dynamics and Monte Carlo simulations of lipid bilayers. *Curr. Opin. Struct. Biol.* **1994**, *4* (4), 486−492.

(7) Vermaas, J. V.; Baylon, J. L.; Arcario, M. J.; Muller, M. P.; Wu, Z.; Pogorelov, T. V.; Tajkhorshid, E. Efficient Exploration of Membrane-Associated Phenomena at Atomic Resolution. *J. Membr. Biol.* **2015**, *248* (3), 563−582.

(8) Chavent, M.; Duncan, A. L.; Sansom, M. S. P. Molecular dynamics simulations of membrane proteins and their interactions: from nanoscale to mesoscale. *Curr. Opin. Struct. Biol.* **2016**, *40*, 8−16.

(9) Marrink, S. J.; Corradi, V.; Souza, P. C. T.; Ingólfsson, H. I.; Tieleman, D. P.; Sansom, M. S. P. Computational Modeling of Realistic Cell Membranes. *Chem. Rev.* **2019**, *119* (9), 6184−6226.

(10) Im, W.; Khalid, S. Molecular Simulations of Gram-Negative Bacterial Membranes Come of Age. *Annu. Rev. Phys. Chem.* **2020**, *71* (1), 171−188.

(11) Aronica, P. G. A.; Reid, L. M.; Desai, N.; Li, J.; Fox, S. J.; Yadahalli, S.; Essex, J. W.; Verma, C. S. Computational Methods and Tools in Antimicrobial Peptide Research. *J. Chem. Inf. Model.* **2021**, *61* (7), 3172−3196.

(12) Ingólfsson, H. I.; Arnarez, C.; Periole, X.; Marrink, S. J. Computational 'microscopy' of cellular membranes. *J. Cell. Sci.* **2016**, *129* (2), 257−268.

(13) Park, S.; Im, W. Quantitative Characterization of Cholesterol Partitioning between Binary Bilayers. *J. Chem. Theory Comput.* **2018**, *14* (6), 2829−2833.

(14) Lee, J.; Patel, D. S.; Kucharska, I.; Tamm, L. K.; Im, W. Refinement of OprH-LPS Interactions by Molecular Simulations. *Biophys. J.* **2017**, *112* (2), 346−355.

(15) Sabin, J.; Alatorre-Meda, M.; Miñones, J.; Domínguez-Arca, V.; Prieto, G. New insights on the mechanism of polyethylenimine transfection and their implications on gene therapy and DNA vaccines. *Colloids Surf., B* **2022**, *210*, 112219.

(16) Park, S.; Choi, Y. K.; Kim, S.; Lee, J.; Im, W. CHARMM-GUI Membrane Builder for Lipid Nanoparticles with Ionizable Cationic Lipids and PEGylated Lipids. *J. Chem. Inf. Model.* **2021**, *61* (10), 5192−5202.

(17) Allsopp, R.; Pavlova, A.; Cline, T.; Salyapongse, A. M.; Gillilan, R. E.; Di, Y. P.; Deslouches, B.; Klauda, J. B.; Gumbart, J. C.; Tristram-Nagle, S. Antimicrobial Peptide Mechanism Studied by Scattering-Guided Molecular Dynamics Simulation. *J. Phys. Chem. B* **2022**, *126* (36), 6922−6935.

(18) Fatafta, H.; Khaled, M.; Owen, M. C.; Sayyed-Ahmad, A.; Strodel, B. Amyloid-β peptide dimers undergo a random coil to β-sheet transition in the aqueous phase but not at the neuronal membrane. *Proc. Natl. Acad. Sci. U. S. A.* **2021**, *118* (39), e2106210118.

(19) Choi, Y. K.; Cao, Y.; Frank, M.; Woo, H.; Park, S.-J.; Yeom, M. S.; Croll, T. I.; Seok, C.; Im, W. Structure, Dynamics, Receptor Binding, and Antibody Binding of the Fully Glycosylated Full-Length SARS-CoV-2 Spike Protein in a Viral Membrane. *J. Chem. Theory Comput.* **2021**, *17* (4), 2479−2487.

(20) Jean, B.; Surratt, C. K.; Madura, J. D. Molecular dynamics of conformation-specific dopamine transporter-inhibitor complexes. *J. Mol. Graph. Model.* **2017**, *76*, 143−151.

(21) Al Kury, L. T.; Papandreou, D.; Hurmach, V. V.; Dryn, D. O.; Melnyk, M. I.; Platonov, M. O.; Prylutskyy, Y. I.; Ritter, U.; Scharff, P.; Zholos, A. V. Single-Walled Carbon Nanotubes Inhibit TRPC4-Mediated Muscarinic Cation Current in Mouse Ileal Myocytes. *Nanomaterials* **2021**, *11* (12), 3410.

(22) Mann, D.; Fan, J.; Somboon, K.; Farrell, D. P.; Muenks, A.; Tzokov, S. B.; DiMaio, F.; Khalid, S.; Miller, S. I.; Bergeron, J. R. C. Structure and lipid dynamics in the maintenance of lipid asymmetry inner membrane complex of *A. baumannii*. *Commun. Biol.* **2021**, *4* (1), 817.

(23) Heberle, F. A.; Myles, D. A. A.; Katsaras, J. Biomembranes research using thermal and cold neutrons. *Chem. Phys. Lipids* **2015**, *192*, 41−50.

(24) van der Wel, P. C. A. Lipid Dynamics and Protein−Lipid Interactions in Integral Membrane Proteins: Insights from Solid-State NMR. *eMagRes.* **2014**, *3*, 111−118.
(25) Lyman, E.; Hsieh, C.-L.; Eggeling, C. From Dynamics to Membrane Organization: Experimental Breakthroughs Occasion a "Modeling Manifesto. *Biophys. J.* **2018**, *115* (4), 595−604.
(26) Cheng, Y. Single-particle cryo-EM—How did it get here and where will it go. *Science* **2018**, *361* (6405), 876−880.
(27) Kühlbrandt, W. Forty years in cryoEM of membrane proteins. *Microscopy* **2022**, *71* (Supplement_1), i30−i50.
(28) Jo, S.; Lim, J. B.; Klauda, J. B.; Im, W. CHARMM-GUI Membrane Builder for Mixed Bilayers and Its Application to Yeast Membranes. *Biophys. J.* **2009**, *97* (1), 50−58.
(29) Klauda, J. B.; Venable, R. M.; Freites, J. A.; O'Connor, J. W.; Tobias, D. J.; Mondragon-Ramirez, C.; Vorobyov, I.; MacKerell, A. D., Jr.; Pastor, R. W. Update of the CHARMM All-Atom Additive Force Field for Lipids: Validation on Six Lipid Types. *J. Phys. Chem. B* **2010**, *114* (23), 7830−7843.
(30) Marrink, S. J.; Risselada, H. J.; Yefimov, S.; Tieleman, D. P.; de Vries, A. H. The MARTINI Force Field: Coarse Grained Model for Biomolecular Simulations. *J. Phys. Chem. B* **2007**, *111* (27), 7812−7824.
(31) Alexander, S. P. H.; Kelly, E.; Mathie, A.; Peters, J. A.; Veale, E. L.; Armstrong, J. F.; Faccenda, E.; Harding, S. D.; Pawson, A. J.; Southan, C.; Buneman, O. P.; Cidlowski, J. A.; Christopoulos, A.; Davenport, A. P.; Fabbro, D.; Spedding, M.; Striessnig, J.; Davies, J. A.; Ahlers-Dannen, K. E.; Alqinyah, M.; Arumugam, T. V.; Bodle, C.; Dagner, J. B.; Chakravarti, B.; Choudhuri, S. P.; Druey, K. M.; Fisher, R. A.; Gerber, K. J.; Hepler, J. R.; Hooks, S. B.; Kantheti, H. S.; Karaj, B.; Layeghi-Ghalehsoukhteh, S.; Lee, J.-K.; Luo, Z.; Martemyanov, K.; Mascarenhas, L. D.; McNabb, H.; Montañez-Miranda, C.; Ogujiofor, O.; Phan, H.; Roman, D. L.; Shaw, V.; Sjogren, B.; Sobey, C.; Spicer, M. M.; Squires, K. E.; Sutton, L.; Wendimu, M.; Wilkie, T.; Xie, K.; Zhang, Q.; Zolghadri, Y. THE CONCISE GUIDE TO PHARMACOLOGY 2021/22: Introduction and Other Protein Targets. *Br. J. Pharmacol.* **2021**, *178* (S1), S1−S26.
(32) Jumper, J.; Evans, R.; Pritzel, A.; Green, T.; Figurnov, M.; Ronneberger, O.; Tunyasuvunakool, K.; Bates, R.; Žídek, A.; Potapenko, A.; Bridgland, A.; Meyer, C.; Kohl, S. A. A.; Ballard, A. J.; Cowie, A.; Romera-Paredes, B.; Nikolov, S.; Jain, R.; Adler, J.; Back, T.; Petersen, S.; Reiman, D.; Clancy, E.; Zielinski, M.; Steinegger, M.; Pacholska, M.; Berghammer, T.; Bodenstein, S.; Silver, D.; Vinyals, O.; Senior, A. W.; Kavukcuoglu, K.; Kohli, P.; Hassabis, D. Highly accurate protein structure prediction with AlphaFold. *Nature* **2021**, *596* (7873), 583−589.
(33) Baek, M.; DiMaio, F.; Anishchenko, I.; Dauparas, J.; Ovchinnikov, S.; Lee, G. R.; Wang, J.; Cong, Q.; Kinch, L. N.; Schaeffer, R. D.; Millán, C.; Park, H.; Adams, C.; Glassman, C. R.; DeGiovanni, A.; Pereira, J. H.; Rodrigues, A. V.; van Dijk, A. A.; Ebrecht, A. C.; Opperman, D. J.; Sagmeister, T.; Buhlheller, C.; Pavkov-Keller, T.; Rathinaswamy, M. K.; Dalwadi, U.; Yip, C. K.; Burke, J. E.; Garcia, K. C.; Grishin, N. V.; Adams, P. D.; Read, R. J.; Baker, D. Accurate prediction of protein structures and interactions using a three-track neural network. *Science* **2021**, *373* (6557), 871−876.
(34) Śledź, P.; Caflisch, A. Protein structure-based drug design: from docking to molecular dynamics. *Curr. Opin. Struct. Biol.* **2018**, *48*, 93−102.
(35) Jo, S.; Cheng, X.; Lee, J.; Kim, S.; Park, S.-J.; Patel, D. S.; Beaven, A. H.; Lee, K. I.; Rui, H.; Park, S.; Lee, H. S.; Roux, B.; MacKerell, A. D., Jr; Klauda, J. B.; Qi, Y.; Im, W. CHARMM-GUI 10 years for biomolecular modeling and simulation. *J. Comput. Chem.* **2017**, *38* (15), 1114−1124.
(36) Jo, S.; Kim, T.; Iyer, V. G.; Im, W. CHARMM-GUI: A web-based graphical user interface for CHARMM. *J. Comput. Chem.* **2008**, *29* (11), 1859−1865.
(37) Jo, S.; Kim, T.; Im, W. Automated Builder and Database of Protein/Membrane Complexes for Molecular Dynamics Simulations. *PLoS One* **2007**, *2* (9), e880.
(38) Lee, J.; Patel, D. S.; Ståhle, J.; Park, S.-J.; Kern, N. R.; Kim, S.; Lee, J.; Cheng, X.; Valvano, M. A.; Holst, O.; Knirel, Y. A.; Qi, Y.; Jo, S.; Klauda, J. B.; Widmalm, G.; Im, W. CHARMM-GUI Membrane Builder for Complex Biological Membrane Simulations with Glycolipids and Lipoglycans. *J. Chem. Theory Comput.* **2019**, *15* (1), 775−786.
(39) Park, S.; Im, W.; Pastor, R. W. Developing initial conditions for simulations of asymmetric membranes: a practical recommendation. *Biophys. J.* **2021**, *120* (22), 5041−5059.
(40) Choi, Y. K.; Kern, N. R.; Kim, S.; Kanhaiya, K.; Afshar, Y.; Jeon, S. H.; Jo, S.; Brooks, B. R.; Lee, J.; Tadmor, E. B.; Heinz, H.; Im, W. CHARMM-GUI Nanomaterial Modeler for Modeling and Simulation of Nanomaterial Systems. *J. Chem. Theory Comput.* **2022**, *18* (1), 479−493.
(41) Choi, Y. K.; Park, S.-J.; Park, S.; Kim, S.; Kern, N. R.; Lee, J.; Im, W. CHARMM-GUI Polymer Builder for Modeling and Simulation of Synthetic Polymers. *J. Chem. Theory Comput.* **2021**, *17* (4), 2431−2443.
(42) Jo, S.; Cheng, X.; Islam, S. M.; Huang, L.; Rui, H.; Zhu, A.; Lee, H. S.; Qi, Y.; Han, W.; Vanommeslaeghe, K.; MacKerell, A. D.; Roux, B.; Im, W. Chapter Eight - CHARMM-GUI PDB Manipulator for Advanced Modeling and Simulations of Proteins Containing Non-standard Residues. In *Advances in Protein Chemistry and Structural Biology*, Karabencheva-Christova, T., Ed.; Academic Press: 2014; Vol. *96*, pp 235−265.
(43) Jo, S.; Jiang, W.; Lee, H. S.; Roux, B. t.; Im, W. CHARMM-GUI Ligand Binder for Absolute Binding Free Energy Calculations and Its Application. *J. Chem. Inf. Model.* **2013**, *53* (1), 267−277.
(44) Kim, S.; Lee, J.; Jo, S.; Brooks, C. L., III; Lee, H. S.; Im, W. CHARMM-GUI ligand reader and modeler for CHARMM force field generation of small molecules. *J. Comput. Chem.* **2017**, *38* (21), 1879−1886.
(45) Kim, S.; Oshima, H.; Zhang, H.; Kern, N. R.; Re, S.; Lee, J.; Roux, B.; Sugita, Y.; Jiang, W.; Im, W. CHARMM-GUI Free Energy Calculator for Absolute and Relative Ligand Solvation and Binding Free Energy Simulations. *J. Chem. Theory Comput.* **2020**, *16* (11), 7207−7218.
(46) Park, S.-J.; Lee, J.; Qi, Y.; Kern, N. R.; Lee, H. S.; Jo, S.; Joung, I.; Joo, K.; Lee, J.; Im, W. CHARMM-GUI Glycan Modeler for modeling and simulation of carbohydrates and glycoconjugates. *Glycobiology* **2019**, *29* (4), 320−331.
(47) Suh, D.; Feng, S.; Lee, H.; Zhang, H.; Park, S.-J.; Kim, S.; Lee, J.; Choi, S.; Im, W. CHARMM-GUI Enhanced Sampler for various collective variables and enhanced sampling methods. *Protein Sci.* **2022**, *31* (11), e4446.
(48) Guterres, H.; Park, S.-J.; Zhang, H.; Perone, T.; Kim, J.; Im, W. CHARMM-GUI high-throughput simulator for efficient evaluation of protein−ligand interactions with different force fields. *Protein Sci.* **2022**, *31* (9), e4413.
(49) Ingólfsson, H. I.; Melo, M. N.; van Eerden, F. J.; Arnarez, C.; Lopez, C. A.; Wassenaar, T. A.; Periole, X.; de Vries, A. H.; Tieleman, D. P.; Marrink, S. J. Lipid Organization of the Plasma Membrane. *J. Am. Chem. Soc.* **2014**, *136* (41), 14554−14559.
(50) Wassenaar, T. A.; Ingólfsson, H. I.; Böckmann, R. A.; Tieleman, D. P.; Marrink, S. J. Computational Lipidomics with insane: A Versatile Tool for Generating Custom Membranes for Molecular Simulations. *J. Chem. Theory Comput.* **2015**, *11* (5), 2144−2155.
(51) Martínez, L.; Andrade, R.; Birgin, E. G.; Martínez, J. M. PACKMOL: A package for building initial configurations for molecular dynamics simulations. *J. Comput. Chem.* **2009**, *30* (13), 2157−2164.
(52) Sommer, B.; Dingersen, T.; Gamroth, C.; Schneider, S. E.; Rubert, S.; Krüger, J.; Dietz, K.-J. CELLmicrocosmos 2.2 MembraneEditor: A Modular Interactive Shape-Based Software Approach To Solve Heterogeneous Membrane Packing Problems. *J. Chem. Inf. Model.* **2011**, *51* (5), 1165−1182.
(53) Boyd, K. J.; May, E. R. BUMPy: A Model-Independent Tool for Constructing Lipid Bilayers of Varying Curvature and Composition. *J. Chem. Theory Comput.* **2018**, *14* (12), 6642−6652.

(54) Durrant, J. D.; Amaro, R. E. LipidWrapper: An Algorithm for Generating Large-Scale Membrane Models of Arbitrary Geometry. *PLoS Comput. Biol.* **2014**, *10* (7), e1003720.
(55) Pezeshkian, W.; König, M.; Wassenaar, T. A.; Marrink, S. J. Backmapping triangulated surfaces to coarse-grained membrane models. *Nat. Commun.* **2020**, *11* (1), 2296.
(56) Johnson, G. T.; Autin, L.; Al-Alusi, M.; Goodsell, D. S.; Sanner, M. F.; Olson, A. J. cellPACK: a virtual mesoscope to model and visualize structural systems biology. *Nat. Methods* **2015**, *12* (1), 85−91.
(57) Johnson, G. T.; Goodsell, D. S.; Autin, L.; Forli, S.; Sanner, M. F.; Olson, A. J. 3D molecular models of whole HIV-1 virions generated with cellPACK. *Faraday Discuss.* **2014**, *169* (0), 23−44.
(58) Maritan, M.; Autin, L.; Karr, J.; Covert, M. W.; Olson, A. J.; Goodsell, D. S. Building Structural Models of a Whole Mycoplasma Cell. *J. Mol. Biol.* **2022**, *434* (2), 167351.
(59) Kjølbye, L. R.; De Maria, L.; Wassenaar, T. A.; Abdizadeh, H.; Marrink, S. J.; Ferkinghoff-Borg, J.; Schiøtt, B. General Protocol for Constructing Molecular Models of Nanodiscs. *J. Chem. Inf. Model.* **2021**, *61* (6), 2869−2883.
(60) Cheng, X.; Jo, S.; Lee, H. S.; Klauda, J. B.; Im, W. CHARMM-GUI Micelle Builder for Pure/Mixed Micelle and Protein/Micelle Complex Systems. *J. Chem. Inf. Model.* **2013**, *53* (8), 2171−2180.
(61) Wu, E. L.; Cheng, X.; Jo, S.; Rui, H.; Song, K. C.; Dávila-Contreras, E. M.; Qi, Y.; Lee, J.; Monje-Galvan, V.; Venable, R. M.; Klauda, J. B.; Im, W. CHARMM-GUI Membrane Builder toward realistic biological membrane simulations. *J. Comput. Chem.* **2014**, *35* (27), 1997−2004.
(62) Qi, Y.; Cheng, X.; Lee, J.; Vermaas, J. V.; Pogorelov, T. V.; Tajkhorshid, E.; Park, S.; Klauda, Jeffery B.; Im, W. CHARMM-GUI HMMM Builder for Membrane Simulations with the Highly Mobile Membrane-Mimetic Model. *Biophys. J.* **2015**, *109* (10), 2012−2022.
(63) Qi, Y.; Ingólfsson, H. I.; Cheng, X.; Lee, J.; Marrink, S. J.; Im, W. CHARMM-GUI Martini Maker for Coarse-Grained Simulations with the Martini Force Field. *J. Chem. Theory Comput.* **2015**, *11* (9), 4486−4494.
(64) Qi, Y.; Lee, J.; Klauda, J. B.; Im, W. CHARMM-GUI Nanodisc Builder for modeling and simulation of various nanodisc systems. *J. Comput. Chem.* **2019**, *40* (7), 893−899.
(65) Monticelli, L.; Kandasamy, S. K.; Periole, X.; Larson, R. G.; Tieleman, D. P.; Marrink, S.-J. The MARTINI Coarse-Grained Force Field: Extension to Proteins. *J. Chem. Theory Comput.* **2008**, *4* (5), 819−834.
(66) Hsu, P.-C.; Bruininks, B. M. H.; Jefferies, D.; Cesar Telles de Souza, P.; Lee, J.; Patel, D. S.; Marrink, S. J.; Qi, Y.; Khalid, S.; Im, W. CHARMM-GUI Martini Maker for modeling and simulation of complex bacterial membranes with lipopolysaccharides. *J. Comput. Chem.* **2017**, *38* (27), 2354−2363.
(67) Ohkubo, Y. Z.; Pogorelov, T. V.; Arcario, M. J.; Christensen, G. A.; Tajkhorshid, E. Accelerating Membrane Insertion of Peripheral Proteins with a Novel Membrane Mimetic Model. *Biophys. J.* **2012**, *102* (9), 2130−2139.
(68) Lee, J.; Cheng, X.; Swails, J. M.; Yeom, M. S.; Eastman, P. K.; Lemkul, J. A.; Wei, S.; Buckner, J.; Jeong, J. C.; Qi, Y.; Jo, S.; Pande, V. S.; Case, D. A.; Brooks, C. L., III; MacKerell, A. D., Jr.; Klauda, J. B.; Im, W. CHARMM-GUI Input Generator for NAMD, GROMACS, AMBER, OpenMM, and CHARMM/OpenMM Simulations Using the CHARMM36 Additive Force Field. *J. Chem. Theory Comput.* **2016**, *12* (1), 405−413.
(69) Lee, J.; Hitzenberger, M.; Rieger, M.; Kern, N. R.; Zacharias, M.; Im, W. CHARMM-GUI supports the Amber force fields. *J. Chem. Phys.* **2020**, *153* (3), No. 035103.
(70) Kognole, A. A.; Lee, J.; Park, S.-J.; Jo, S.; Chatterjee, P.; Lemkul, J. A.; Huang, J.; MacKerell, A. D., Jr.; Im, W. CHARMM-GUI Drude prepper for molecular dynamics simulation using the classical Drude polarizable force field. *J. Comput. Chem.* **2022**, *43* (5), 359−375.
(71) Park, S.-J.; Kern, N.; Brown, T.; Lee, J.; Im, W. CHARMM-GUI PDB Manipulator: Various PDB Structural Modifications for Biomolecular Modeling and Simulation. *J. Mol. Biol.* **2023**, 167995.
(72) Woolf, T. B.; Roux, B. Structure, energetics, and dynamics of lipid−protein interactions: A molecular dynamics study of the gramicidin A channel in a DMPC bilayer. *Proteins: Struct., Funct., Bioinf.* **1996**, *24* (1), 92−114.
(73) Vácha, R.; Berkowitz, M. L.; Jungwirth, P. Molecular Model of a Cell Plasma Membrane With an Asymmetric Multicomponent Composition: Water Permeation and Ion Effects. *Biophys. J.* **2009**, *96* (11), 4493−4501.
(74) Pogozheva, I. D.; Armstrong, G. A.; Kong, L.; Hartnagel, T. J.; Carpino, C. A.; Gee, S. E.; Picarello, D. M.; Rubin, A. S.; Lee, J.; Park, S.; Lomize, A. L.; Im, W. Comparative Molecular Dynamics Simulation Studies of Realistic Eukaryotic, Prokaryotic, and Archaeal Membranes. *J. Chem. Inf. Model.* **2022**, *62* (4), 1036−1051.
(75) Feng, S.; Kong, L.; Gee, S.; Im, W. Molecular Condensate in a Membrane: A Tugging Game between Hydrophobicity and Polarity with Its Biological Significance. *Langmuir* **2022**, *38* (19), 5955−5962.
(76) Harayama, T.; Riezman, H. Understanding the diversity of membrane lipid composition. *Nat. Rev. Mol. Cell Biol.* **2018**, *19* (5), 281−296.
(77) van Meer, G.; Voelker, D. R.; Feigenson, G. W. Membrane lipids: where they are and how they behave. *Nat. Rev. Mol. Cell Biol.* **2008**, *9* (2), 112−124.
(78) Kaneda, T. Iso- and anteiso-fatty acids in bacteria: biosynthesis, function, and taxonomic significance. *Microbiol. Rev.* **1991**, *55* (2), 288−302.
(79) Sohlenkamp, C.; Geiger, O. Bacterial membrane lipids: diversity in structures and pathways. *FEMS Microbiol. Rev.* **2016**, *40* (1), 133−159.
(80) Dufourc, E. J.; Smith, I. C. P.; Jarrell, H. C. The role of cyclopropane moieties in the lipid properties of biological membranes: a deuterium NMR structural and dynamical approach. *Biochemistry* **1984**, *23* (10), 2300−2309.
(81) Grogan, D. W.; Cronan, J. E. Cyclopropane ring formation in membrane lipids of bacteria. *Microbiol. Mol. Biol. Rev.* **1997**, *61* (4), 429−441.
(82) Akira, S.; Uematsu, S.; Takeuchi, O. Pathogen Recognition and Innate Immunity. *Cell* **2006**, *124* (4), 783−801.
(83) Raetz, C. R. H.; Whitfield, C. Lipopolysaccharide Endotoxins. *Annu. Rev. Biochem.* **2002**, *71* (1), 635−700.
(84) Ruiz, N.; Kahne, D.; Silhavy, T. J. Advances in understanding bacterial outer-membrane biogenesis. *Nat. Rev. Microbiol.* **2006**, *4* (1), 57−66.
(85) Caforio, A.; Driessen, A. J. M. Archaeal phospholipids: Structural properties and biosynthesis. *Biochim. Biophys. Acta, Mol. Cell Biol. Lipids* **2017**, *1862* (11), 1325−1339.
(86) Ghani, L.; Kim, S.; Wang, H.; Lee, H. S.; Mortensen, J. S.; Katsube, S.; Du, Y.; Sadaf, A.; Ahmed, W.; Byrne, B.; Guan, L.; Loland, C. J.; Kobilka, B. K.; Im, W.; Chae, P. S. Foldable Detergents for Membrane Protein Study: Importance of Detergent Core Flexibility in Protein Stabilization. *Chem. Eur. J.* **2022**, *28* (21), e202200116.
(87) Parker, J. L.; Newstead, S. Current trends in α-helical membrane protein crystallization: An update. *Protein Sci.* **2012**, *21* (9), 1358−1365.
(88) Privé, G. G. Detergents for the stabilization and crystallization of membrane proteins. *Methods* **2007**, *41* (4), 388−397.
(89) Sadaf, A.; Kim, S.; Bae, H. E.; Wang, H.; Nygaard, A.; Uegaki, Y.; Du, Y.; Munk, C. F.; Katsube, S.; Sung Lee, H.; Bae, J.; Choi, C. W.; Choi, H.-J.; Byrne, B.; Gellman, S. H.; Guan, L.; Loland, C. J.; Kobilka, B. K.; Im, W.; Chae, P. S. Conformationally flexible core-bearing detergents with a hydrophobic or hydrophilic pendant: Effect of pendant polarity on detergent conformation and membrane protein stability. *Acta Biomater.* **2021**, *128*, 393−407.
(90) Cullis, P. R.; Hope, M. J. Lipid Nanoparticle Systems for Enabling Gene Therapies. *Mol. Ther.* **2017**, *25* (7), 1467−1475.

https://doi.org/10.1021/acs.jctc.2c01246
J. Chem. Theory Comput. 2023, 19, 2161−2185

(91) Evers, M. J. W.; Kulkarni, J. A.; van der Meel, R.; Cullis, P. R.; Vader, P.; Schiffelers, R. M. State-of-the-Art Design and Rapid-Mixing Production Techniques of Lipid Nanoparticles for Nucleic Acid Delivery. *Small Methods* **2018**, *2* (9), 1700375.
(92) Jayaraman, M.; Ansell, S. M.; Mui, B. L.; Tam, Y. K.; Chen, J.; Du, X.; Butler, D.; Eltepu, L.; Matsuda, S.; Narayanannair, J. K.; Rajeev, K. G.; Hafez, I. M.; Akinc, A.; Maier, M. A.; Tracy, M. A.; Cullis, P. R.; Madden, T. D.; Manoharan, M.; Hope, M. J. Maximizing the Potency of siRNA Lipid Nanoparticles for Hepatic Gene Silencing In Vivo**. *Angew. Chem., Int. Ed.* **2012**, *51* (34), 8529−8533.
(93) Lechanteur, A.; Furst, T.; Evrard, B.; Delvenne, P.; Hubert, P.; Piel, G. PEGylation of lipoplexes: The right balance between cytotoxicity and siRNA effectiveness. *Eur. J. Pharm. Sci.* **2016**, *93*, 493−503.
(94) Song, L. Y.; Ahkong, Q. F.; Rong, Q.; Wang, Z.; Ansell, S.; Hope, M. J.; Mui, B. Characterization of the inhibitory effect of PEG-lipid conjugates on the intracellular delivery of plasmid and antisense DNA mediated by cationic lipid liposomes. *Biochim. Biophys. Acta, Biomembr.* **2002**, *1558* (1), 1−13.
(95) Pike, L. J. Rafts defined: a report on the Keystone symposium on lipid rafts and cell function. *J. Lipid Res.* **2006**, *47* (7), 1597−1598.
(96) Simons, K.; Sampaio, J. L. Membrane Organization and Lipid Rafts. *Cold Spring Harbor Perspect. Biol.* **2011**, *3* (10), a004697.
(97) Sezgin, E.; Levental, I.; Mayor, S.; Eggeling, C. The mystery of membrane organization: composition, regulation and roles of lipid rafts. *Nat. Rev. Mol. Cell Biol.* **2017**, *18* (6), 361−374.
(98) Feigenson, G. W. Phase diagrams and lipid domains in multicomponent lipid bilayer mixtures. *Biochim. Biophys. Acta, Biomembr.* **2009**, *1788* (1), 47−52.
(99) Goh, S. L.; Amazon, J. J.; Feigenson, G. W. Toward a Better Raft Model: Modulated Phases in the Four-Component Bilayer, DSPC/DOPC/POPC/CHOL. *Biophys. J.* **2013**, *104* (4), 853−862.
(100) Heberle, F. A.; Wu, J.; Goh, S. L.; Petruzielo, R. S.; Feigenson, G. W. Comparison of Three Ternary Lipid Bilayer Mixtures: FRET and ESR Reveal Nanodomains. *Biophys. J.* **2010**, *99* (10), 3309−3318.
(101) Konyakhina, T. M.; Goh, S. L.; Amazon, J.; Heberle, F. A.; Wu, J.; Feigenson, G. W. Control of a Nanoscopic-to-Macroscopic Transition: Modulated Phases in Four-Component DSPC/DOPC/POPC/Chol Giant Unilamellar Vesicles. *Biophys. J.* **2011**, *101* (2), L8−L10.
(102) Zhao, J.; Wu, J.; Heberle, F. A.; Mills, T. T.; Klawitter, P.; Huang, G.; Costanza, G.; Feigenson, G. W. Phase studies of model biomembranes: Complex behavior of DSPC/DOPC/Cholesterol. *Biochim. Biophys. Acta, Biomembr.* **2007**, *1768* (11), 2764−2776.
(103) Veatch, S. L.; Cicuta, P.; Sengupta, P.; Honerkamp-Smith, A.; Holowka, D.; Baird, B. Critical Fluctuations in Plasma Membrane Vesicles. *ACS Chem. Biol.* **2008**, *3* (5), 287−293.
(104) Levental, I.; Grzybek, M.; Simons, K. Raft domains of variable properties and compositions in plasma membrane vesicles. *Proc. Natl. Acad. Sci. U. S. A.* **2011**, *108* (28), 11411−11416.
(105) Ackerman, D. G.; Feigenson, G. W. Multiscale Modeling of Four-Component Lipid Mixtures: Domain Composition, Size, Alignment, and Properties of the Phase Interface. *J. Phys. Chem. B* **2015**, *119* (11), 4240−4250.
(106) Baoukina, S.; Mendez-Villuendas, E.; Bennett, W. F. D.; Tieleman, D. P. Computer simulations of the phase separation in model membranes. *Faraday Discuss.* **2013**, *161* (0), 63−75.
(107) Bennett, W. F. D.; Shea, J.-E.; Tieleman, D. P. Phospholipid Chain Interactions with Cholesterol Drive Domain Formation in Lipid Membranes. *Biophys. J.* **2018**, *114* (11), 2595−2605.
(108) Carpenter, T. S.; López, C. A.; Neale, C.; Montour, C.; Ingólfsson, H. I.; Di Natale, F.; Lightstone, F. C.; Gnanakaran, S. Capturing Phase Behavior of Ternary Lipid Mixtures with a Refined Martini Coarse-Grained Force Field. *J. Chem. Theory Comput.* **2018**, *14* (11), 6050−6062.
(109) Hakobyan, D.; Heuer, A. Phase Separation in a Lipid/Cholesterol System: Comparison of Coarse-Grained and United-Atom Simulations. *J. Phys. Chem. B* **2013**, *117* (14), 3841−3851.
(110) Kučerka, N.; Marquardt, D.; Harroun, T. A.; Nieh, M.-P.; Wassall, S. R.; de Jong, D. H.; Schäfer, L. V.; Marrink, S. J.; Katsaras, J. Cholesterol in Bilayers with PUFA Chains: Doping with DMPC or POPC Results in Sterol Reorientation and Membrane-Domain Formation. *Biochemistry* **2010**, *49* (35), 7485−7493.
(111) Risselada, H. J.; Marrink, S. J. The molecular face of lipid rafts in model membranes. *Proc. Natl. Acad. Sci. U. S. A.* **2008**, *105* (45), 17367−17372.
(112) Rosetti, C.; Pastorino, C. Polyunsaturated and Saturated Phospholipids in Mixed Bilayers: A Study from the Molecular Scale to the Lateral Lipid Organization. *J. Phys. Chem. B* **2011**, *115* (5), 1002−1013.
(113) Wang, Y.; Gkeka, P.; Fuchs, J. E.; Liedl, K. R.; Cournia, Z. DPPC-cholesterol phase diagram using coarse-grained Molecular Dynamics simulations. *Biochim. Biophys. Acta, Biomembr.* **2016**, *1858* (11), 2846−2857.
(114) Javanainen, M.; Martinez-Seara, H.; Vattulainen, I. Nanoscale Membrane Domain Formation Driven by Cholesterol. *Sci. Rep.* **2017**, *7* (1), 1143.
(115) Sodt, A.J.; Pastor, R. W.; Lyman, E. Hexagonal Substructure and Hydrogen Bonding in Liquid-Ordered Phases Containing Palmitoyl Sphingomyelin. *Biophys. J.* **2015**, *109* (5), 948−955.
(116) Sodt, A. J.; Sandar, M. L.; Gawrisch, K.; Pastor, R. W.; Lyman, E. The Molecular Structure of the Liquid-Ordered Phase of Lipid Bilayers. *J. Am. Chem. Soc.* **2014**, *136* (2), 725−732.
(117) Kinoshita, M.; Yamaguchi, S.; Matsumori, N. Low-flux scanning electron diffraction reveals substructures inside the ordered membrane domain. *Sci. Rep.* **2020**, *10* (1), 22188.
(118) Unguryan, V. V.; Golysheva, E. A.; Dzuba, S. A. Double Electron−Electron Resonance of Spin-Labeled Cholestane in Model Membranes: Evidence for Substructures inside the Lipid Rafts. *J. Phys. Chem. B* **2021**, *125* (33), 9557−9563.
(119) Ghysels, A.; Krämer, A.; Venable, R. M.; Teague, W. E.; Lyman, E.; Gawrisch, K.; Pastor, R. W. Permeability of membranes in the liquid ordered and liquid disordered phases. *Nat. Commun.* **2019**, *10* (1), 5616.
(120) Aittoniemi, J.; Niemelä, P. S.; Hyvönen, M. T.; Karttunen, M.; Vattulainen, I. Insight into the Putative Specific Interactions between Cholesterol, Sphingomyelin, and Palmitoyl-Oleoyl Phosphatidylcholine. *Biophys. J.* **2007**, *92* (4), 1125−1137.
(121) Leventis, R.; Silvius, J. R. Use of Cyclodextrins to Monitor Transbilayer Movement and Differential Lipid Affinities of Cholesterol. *Biophys. J.* **2001**, *81* (4), 2257−2267.
(122) Niu, S.-L.; Litman, B. J. Determination of Membrane Cholesterol Partition Coefficient Using a Lipid Vesicle−Cyclodextrin Binary System: Effect of Phospholipid Acyl Chain Unsaturation and Headgroup Composition. *Biophys. J.* **2002**, *83* (6), 3408−3415.
(123) Niu, S.-L.; Mitchell, D. C.; Litman, B. J. Manipulation of Cholesterol Levels in Rod Disk Membranes by Methyl-β-cyclodextrin: EFFECTS ON RECEPTOR ACTIVATION*. *J. Biol. Chem.* **2002**, *277* (23), 20139−20145.
(124) Ohvo-Rekilä, H.; Åkerlund, B.; Slotte, J. P. Cyclodextrin-catalyzed extraction of fluorescent sterols from monolayer membranes and small unilamellar vesicles. *Chem. Phys. Lipids* **2000**, *105* (2), 167−178.
(125) Nakagawa, Y.; Inoue, K.; Nojima, S. Transfer of cholesterol between liposomal membranes. *Biochim. Biophys. Acta, Biomembr.* **1979**, *553* (2), 307−319.
(126) Wattenberg, B. W.; Silbert, D. F. Sterol partitioning among intracellular membranes. Testing a model for cellular sterol distribution. *J. Biol. Chem.* **1983**, *258* (4), 2284−2289.
(127) Yeagle, P. L.; Young, J. E. Factors contributing to the distribution of cholesterol among phospholipid vesicles. *J. Biol. Chem.* **1986**, *261* (18), 8175−8181.
(128) Bennett, W. F. D.; MacCallum, J. L.; Hinner, M. J.; Marrink, S. J.; Tieleman, D. P. Molecular View of Cholesterol Flip-Flop and Chemical Potential in Different Membrane Environments. *J. Am. Chem. Soc.* **2009**, *131* (35), 12714−12720.

https://doi.org/10.1021/acs.jctc.2c01246
J. Chem. Theory Comput. 2023, 19, 2161−2185

(129) Zhang, Z.; Lu, L.; Berkowitz, M. L. Energetics of Cholesterol Transfer between Lipid Bilayers. *J. Phys. Chem. B* **2008**, *112* (12), 3807−3811.
(130) López, C. A.; de Vries, A. H.; Marrink, S. J. Molecular Mechanism of Cyclodextrin Mediated Cholesterol Extraction. *PLoS Comput. Biol.* **2011**, *7* (3), e1002020.
(131) López, C. A.; de Vries, A. H.; Marrink, S. J. Computational microscopy of cyclodextrin mediated cholesterol extraction from lipid model membranes. *Sci. Rep.* **2013**, *3* (1), 2071.
(132) Ermilova, I.; Swenson, J. DOPC versus DOPE as a helper lipid for gene-therapies: molecular dynamics simulations with DLin-MC3-DMA. *Phys. Chem. Chem. Phys.* **2020**, *22* (48), 28256−28268.
(133) Ramezanpour, M.; Schmidt, M. L.; Bodnariuc, I.; Kulkarni, J. A.; Leung, S. S. W.; Cullis, P. R.; Thewalt, J. L.; Tieleman, D. P. Ionizable amino lipid interactions with POPC: implications for lipid nanoparticle function. *Nanoscale* **2019**, *11* (30), 14141−14146.
(134) Rizo, J.; Sari, L.; Qi, Y.; Im, W.; Lin, M. M. All-atom molecular dynamics simulations of Synaptotagmin-SNARE-complexin complexes bridging a vesicle and a flat lipid bilayer. *eLife* **2022**, *11*, e76356.
(135) Sutton, R. B.; Fasshauer, D.; Jahn, R.; Brunger, A. T. Crystal structure of a SNARE complex involved in synaptic exocytosis at 2.4 Å resolution. *Nature* **1998**, *395* (6700), 347−353.
(136) Ma, C.; Su, L.; Seven, A. B.; Xu, Y.; Rizo, J. Reconstitution of the Vital Functions of Munc18 and Munc13 in Neurotransmitter Release. *Science* **2013**, *339* (6118), 421−425.
(137) Südhof, T. C. Neurotransmitter Release: The Last Millisecond in the Life of a Synaptic Vesicle. *Neuron* **2013**, *80* (3), 675−690.
(138) Fernández-Chacón, R.; Königstorfer, A.; Gerber, S. H.; García, J.; Matos, M. F.; Stevens, C. F.; Brose, N.; Rizo, J.; Rosenmund, C.; Südhof, T. C. Synaptotagmin I functions as a calcium regulator of release probability. *Nature* **2001**, *410* (6824), 41−49.
(139) Chen, X.; Tomchick, D. R.; Kovrigin, E.; Araç, D.; Machius, M.; Südhof, T. C.; Rizo, J. Three-Dimensional Structure of the Complexin/SNARE Complex. *Neuron* **2002**, *33* (3), 397−409.
(140) Xue, M.; Reim, K.; Chen, X.; Chao, H.-T.; Deng, H.; Rizo, J.; Brose, N.; Rosenmund, C. Distinct domains of complexin I differentially regulate neurotransmitter release. *Nat. Struct. Mol. Biol.* **2007**, *14* (10), 949−958.
(141) Manca, F.; Pincet, F.; Truskinovsky, L.; Rothman, J. E.; Foret, L.; Caruel, M. SNARE machinery is optimized for ultrafast fusion. *Proc. Natl. Acad. Sci. U. S. A.* **2019**, *116* (7), 2435−2442.
(142) McDargh, Z. A.; Polley, A.; O'Shaughnessy, B. SNARE-mediated membrane fusion is a two-stage process driven by entropic forces. *FEBS Lett.* **2018**, *592* (21), 3504−3515.
(143) Mostafavi, H.; Thiyagarajan, S.; Stratton, B. S.; Karatekin, E.; Warner, J. M.; Rothman, J. E.; O'Shaughnessy, B. Entropic forces drive self-organization and membrane fusion by SNARE proteins. *Proc. Natl. Acad. Sci. U. S. A.* **2017**, *114* (21), 5455−5460.
(144) Risselada, H. J.; Kutzner, C.; Grubmüller, H. Caught in the Act: Visualization of SNARE-Mediated Fusion Events in Molecular Detail. *ChemBioChem.* **2011**, *12* (7), 1049−1055.
(145) Sharma, S.; Lindau, M. Molecular mechanism of fusion pore formation driven by the neuronal SNARE complex. *Proc. Natl. Acad. Sci. U. S. A.* **2018**, *115* (50), 12751−12756.
(146) Napolitano, F.; Xu, X.; Gao, X. Impact of computational approaches in the fight against COVID-19: an AI guided review of 17 000 studies. *Brief. Bioinformatics* **2022**, *23* (1), bbab456.
(147) Sahoo, M. B.; Bhattamisra, K. S.; Das, S.; Tiwari, A.; Tiwari, V.; Kumar, M.; Singh, S. Computational Approach to Combat COVID-19 Infection: Emerging Tools for Accelerating Drug Research. *Curr. Drug. Discov. Technol.* **2022**, *19* (3), 40−53.
(148) Rosenbaum, D. M.; Rasmussen, S. G.; Kobilka, B. K. The structure and function of G-protein-coupled receptors. *Nature* **2009**, *459* (7245), 356−63.
(149) Azam, S.; Haque, M. E.; Jakaria, M.; Jo, S.-H.; Kim, I.-S.; Choi, D.-K. G-Protein-Coupled Receptors in CNS: A Potential Therapeutic Target for Intervention in Neurodegenerative Disorders and Associated Cognitive Deficits. *Cells* **2020**, *9* (2), 506.
(150) Kharche, S.; Joshi, M.; Chattopadhyay, A.; Sengupta, D. Conformational plasticity and dynamic interactions of the N-terminal domain of the chemokine receptor CXCR1. *PLoS Comput. Biol.* **2021**, *17* (5), e1008593.
(151) Lambey, P.; Otun, O.; Cong, X.; Hoh, F.; Brunel, L.; Verdié, P.; Grison, C. M.; Peysson, F.; Jeannot, S.; Durroux, T.; Bechara, C.; Granier, S.; Leyrat, C. Structural insights into recognition of chemokine receptors by Staphylococcus aureus leukotoxins. *eLife* **2022**, *11*, e72555.
(152) Park, C.; Kim, J.; Ko, S.-B.; Choi, Y. K.; Jeong, H.; Woo, H.; Kang, H.; Bang, I.; Kim, S. A.; Yoon, T.-Y.; Seok, C.; Im, W.; Choi, H.-J. Structural basis of neuropeptide Y signaling through Y1 receptor. *Nat. Commun.* **2022**, *13* (1), 853.
(153) Silva, S.; Marto, J.; Gonçalves, L. M.; Fernandes, H. S.; Sousa, S. F.; Almeida, A. J.; Vale, N. Development of Neuropeptide Y and Cell-Penetrating Peptide MAP Adsorbed onto Lipid Nanoparticle Surface. *Molecules* **2022**, *27* (9), 2734.
(154) Smit, F. X.; van der Velden, W. J. C.; Kizilkaya, H. S.; Nørskov, A.; Lückmann, M.; Hansen, T. N.; Sparre-Ulrich, A. H.; Qvotrup, K.; Frimurer, T. M.; Rosenkilde, M. M. Investigating GIPR (ant)agonism: A structural analysis of GIP and its receptor. *Structure* **2021**, *29* (7), 679−693.e6.
(155) Zhao, F.; Zhang, C.; Zhou, Q.; Hang, K.; Zou, X.; Chen, Y.; Wu, F.; Rao, Q.; Dai, A.; Yin, W.; Shen, D.-D.; Zhang, Y.; Xia, T.; Stevens, R. C.; Xu, H. E.; Yang, D.; Zhao, L.; Wang, M.-W. Structural insights into hormone recognition by the human glucose-dependent insulinotropic polypeptide receptor. *eLife* **2021**, *10*, e68719.
(156) Cong, Z.; Zhou, F.; Zhang, C.; Zou, X.; Zhang, H.; Wang, Y.; Zhou, Q.; Cai, X.; Liu, Q.; Li, J.; Shao, L.; Mao, C.; Wang, X.; Wu, J.; Xia, T.; Zhao, L.-H.; Jiang, H.; Zhang, Y.; Xu, H. E.; Cheng, X.; Yang, D.; Wang, M.-W. Constitutive signal bias mediated by the human GHRHR splice variant 1. *Proc. Natl. Acad. Sci. U. S. A.* **2021**, *118* (40), e2106606118.
(157) Plouffe, B.; Karamitri, A.; Flock, T.; Gallion, J. M.; Houston, S.; Daly, C. A.; Bonnefond, A.; Guillaume, J.-L.; Le Gouill, C.; Froguel, P.; Lichtarge, O.; Deupi, X.; Jockers, R.; Bouvier, M. Structural Elements Directing G Proteins and β-Arrestin Interactions with the Human Melatonin Type 2 Receptor Revealed by Natural Variants. *ACS Pharmacol. Transl. Sci.* **2022**, *5* (2), 89−101.
(158) Zhao, L.; He, X.; Jiang, H.; Cheng, X. Computational characterization of transducer recognition of β2 adrenergic receptor. *Biochem. Biophys. Res. Commun.* **2022**, *592*, 67−73.
(159) Zhang, L.; Bijker, M. S.; Herzog, H. The neuropeptide Y system: Pathophysiological and therapeutic implications in obesity and cancer. *Pharmacol. Ther.* **2011**, *131* (1), 91−113.
(160) Tasan, R. O.; Nguyen, N. K.; Weger, S.; Sartori, S. B.; Singewald, N.; Heilbronn, R.; Herzog, H.; Sperk, G. The Central and Basolateral Amygdala Are Critical Sites of Neuropeptide Y/Y2 Receptor-Mediated Regulation of Anxiety and Depression. *J. Neurosci.* **2010**, *30* (18), 6282−6290.
(161) Bharathi; Roy, K. K. Structural basis for the binding of a selective inverse agonist AF64394 with the human G-protein coupled receptor 3 (GPR3). *J. Biomol. Struct. Dyn.* **2022**, *40*, 10181.
(162) Wang, X.; Cheng, X.; Zhao, L.; Wang, Y.; Ye, C.; Zou, X.; Dai, A.; Cong, Z.; Chen, J.; Zhou, Q.; Xia, T.; Jiang, H.; Xu, H. E.; Yang, D.; Wang, M.-W. Molecular insights into differentiated ligand recognition of the human parathyroid hormone receptor 2. *Proc. Natl. Acad. Sci. U. S. A.* **2021**, *118* (32), e2101279118.
(163) Xu, Y.; Feng, W.; Zhou, Q.; Liang, A.; Li, J.; Dai, A.; Zhao, F.; Yan, J.; Chen, C.-W.; Li, H.; Zhao, L.-H.; Xia, T.; Jiang, Y.; Xu, H. E.; Yang, D.; Wang, M.-W. A distinctive ligand recognition mechanism by the human vasoactive intestinal polypeptide receptor 2. *Nat. Commun.* **2022**, *13* (1), 2272.
(164) Zhao, W.; Han, S.; Qiu, N.; Feng, W.; Lu, M.; Zhang, W.; Wang, M.; Zhou, Q.; Chen, S.; Xu, W.; Du, J.; Chu, X.; Yi, C.; Dai, A.; Hu, L.; Shen, M. Y.; Sun, Y.; Zhang, Q.; Ma, Y.; Zhong, W.; Yang, D.; Wang, M.-W.; Wu, B.; Zhao, Q. Structural insights into ligand recognition and selectivity of somatostatin receptors. *Cell Res.* **2022**, *32* (8), 761−772.

https://doi.org/10.1021/acs.jctc.2c01246
J. Chem. Theory Comput. 2023, 19, 2161−2185

(165) Lee, Y.; Hou, X.; Lee, J. H.; Nayak, A.; Alexander, V.; Sharma, P. K.; Chang, H.; Phan, K.; Gao, Z.-G.; Jacobson, K. A.; Choi, S.; Jeong, L. S. Subtle Chemical Changes Cross the Boundary between Agonist and Antagonist: New A_3 Adenosine Receptor Homology Models and Structural Network Analysis Can Predict This Boundary. *J. Med. Chem.* **2021**, *64* (17), 12525−12536.
(166) Shiriaeva, A.; Park, D.; Kim, G.; Lee, Y.; Hou, X.; Jarhad, D. B.; Kim, G.; Yu, J.; Hyun, Y. E.; Kim, W.; Gao, Z.-G.; Jacobson, K. A.; Han, G. W.; Stevens, R. C.; Jeong, L. S.; Choi, S.; Cherezov, V. GPCR Agonist-to-Antagonist Conversion: Enabling the Design of Nucleoside Functional Switches for the A_{2A} Adenosine Receptor. *J. Med. Chem.* **2022**, *65* (17), 11648−11657.
(167) Velazhahan, V.; Ma, N.; Vaidehi, N.; Tate, C. G. Activation mechanism of the class D fungal GPCR dimer Ste2. *Nature* **2022**, *603* (7902), 743−748.
(168) Dutta, S.; Selvam, B.; Shukla, D. Distinct Binding Mechanisms for Allosteric Sodium Ion in Cannabinoid Receptors. *ACS Chem. Neurosci.* **2022**, *13* (3), 379−389.
(169) Mhashal, A. R.; Yoluk, O.; Orellana, L. Exploring the Conformational Impact of Glycine Receptor TM1−2 Mutations Through Coarse-Grained Analysis and Atomistic Simulations. *Front. Mol. Biosci.* **2022**, *9*, 890851.
(170) Lambert, E.; Mehdipour, A. R.; Schmidt, A.; Hummer, G.; Perez, C. Evidence for a trap-and-flip mechanism in a proton-dependent lipid transporter. *Nat. Commun.* **2022**, *13* (1), 1022.
(171) Overington, J. P.; Al-Lazikani, B.; Hopkins, A. L. How many drug targets are there? *Nat. Rev. Drug Discov.* **2006**, *5* (12), 993−996.
(172) Dolphin, A. C.; Insel, P. A.; Blaschke, T. F.; Meyer, U. A. Introduction to the Theme "Ion Channels and Neuropharmacology: From the Past to the Future. *Annu. Rev. Pharmacol. Toxicol.* **2020**, *60* (1), 1−6.
(173) Yu, H.-b.; Li, M.; Wang, W.-p.; Wang, X.-l. High throughput screening technologies for ion channels. *Acta Pharmacol. Sin.* **2016**, *37* (1), 34−43.
(174) Alexander, S. P. H.; Mathie, A.; Peters, J. A.; Veale, E. L.; Striessnig, J.; Kelly, E.; Armstrong, J. F.; Faccenda, E.; Harding, S. D.; Pawson, A. J.; Southan, C.; Davies, J. A.; Aldrich, R. W.; Attali, B.; Baggetta, A. M.; Becirovic, E.; Biel, M.; Bill, R. M.; Catterall, W. A.; Conner, A. C.; Davies, P.; Delling, M.; Virgilio, F. D.; Falzoni, S.; Fenske, S.; George, C.; Goldstein, S. A. N.; Grissmer, S.; Ha, K.; Hammelmann, V.; Hanukoglu, I.; Jarvis, M.; Jensen, A. A.; Kaczmarek, L. K.; Kellenberger, S.; Kennedy, C.; King, B.; Kitchen, P.; Lynch, J. W.; Perez-Reyes, E.; Plant, L. D.; Rash, L.; Ren, D.; Salman, M. M.; Sivilotti, L. G.; Smart, T. G.; Snutch, T. P.; Tian, J.; Trimmer, J. S.; Van den Eynde, C.; Vriens, J.; Wei, A. D.; Winn, B. T.; Wulff, H.; Xu, H.; Yue, L.; Zhang, X.; Zhu, M. THE CONCISE GUIDE TO PHARMACOLOGY 2021/22: Ion channels. *Br. J. Pharmacol.* **2021**, *178* (S1), S157−S245.
(175) Damann, N.; Voets, T.; Nilius, B. TRPs in Our Senses. *Curr. Biol.* **2008**, *18* (18), R880−R889.
(176) Numata, T.; Kiyonaka, S.; Kato, K.; Takahashi, N.; Mori, Y. Chapter 3 Activation of TRP Channels in Mammalian Systems. In *TRP Channels*; Zhu, M. X., Ed.; CRC Press/Taylor & Frances: Boca Raton, FL, 2011.
(177) Koivisto, A.-P.; Belvisi, M. G.; Gaudet, R.; Szallasi, A. Advances in TRP channel drug discovery: from target validation to clinical studies. *Nat. Rev. Drug Discov.* **2022**, *21* (1), 41−59.
(178) Behera, B. K.; Parhi, J.; Dehury, B.; Rout, A. K.; Khatei, A.; Devi, A. L.; Mandal, S. C. Molecular characterization and structural dynamics of Aquaporin1 from walking catfish in lipid bilayers. *Int. J. Biol. Macromol.* **2022**, *196*, 86−97.
(179) Jiang, D.; Banh, R.; Gamal El-Din, T. M.; Tonggu, L.; Lenaeus, M. J.; Pomès, R.; Zheng, N.; Catterall, W. A. Open-state structure and pore gating mechanism of the cardiac sodium channel. *Cell* **2021**, *184* (20), 5151−5162.e11.
(180) Yelshanskaya, M. V.; Patel, D. S.; Kottke, C. M.; Kurnikova, M. G.; Sobolevsky, A. I. Opening of glutamate receptor channel to subconductance levels. *Nature* **2022**, *605* (7908), 172−178.
(181) Smart, O. S.; Neduvelil, J. G.; Wang, X.; Wallace, B. A.; Sansom, M. S. P. HOLE: A program for the analysis of the pore dimensions of ion channel structural models. *J. Mol. Graph.* **1996**, *14* (6), 354−360.
(182) Berselli, A.; Alberini, G.; Benfenati, F.; Maragliano, L. Computational Assessment of Different Structural Models for Claudin-5 Complexes in Blood−Brain Barrier Tight Junctions. *ACS Chem. Neurosci.* **2022**, *13* (14), 2140−2153.
(183) Berselli, A.; Alberini, G.; Benfenati, F.; Maragliano, L. Computational study of ion permeation through claudin-4 paracellular channels. *Ann. N.Y. Acad. Sci.* **2022**, *1516* (1), 162−174.
(184) Milenkovic, S.; Bodrenko, I. V.; Carpaneto, A.; Ceccarelli, M. The key role of the central cavity in sodium transport through ligand-gated two-pore channels. *Phys. Chem. Chem. Phys.* **2021**, *23* (34), 18461−18474.
(185) Sun, Z.; Gong, Z.; Xia, F.; He, X. Ion dynamics and selectivity of Nav channels from molecular dynamics simulation. *Chem. Phys.* **2021**, *548*, 111245.
(186) Vallée, C.; Howlin, B. J.; Lewis, R. Single ion free energy calculation in ASIC1: the importance of the HG loop. *Phys. Chem. Chem. Phys.* **2022**, *24* (22), 13824−13830.
(187) Allegrini, B.; Jedele, S.; David Nguyen, L.; Mignotet, M.; Rapetti-Mauss, R.; Etchebest, C.; Fenneteau, O.; Loubat, A.; Boutet, A.; Thomas, C.; Durin, J.; Petit, A.; Badens, C.; Garçon, L.; Da Costa, L.; Guizouarn, H. New KCNN4 Variants Associated With Anemia: Stomatocytosis Without Erythrocyte Dehydration. *Front. Physiol.* **2022**, *13*, 918620.
(188) Hung, A.; Forster, I. C.; McKenzie, C. E.; Berecki, G.; Petrou, S.; Kathirvel, A.; Soh, M. S.; Reid, C. A. Biophysical analysis of an HCN1 epilepsy variant suggests a critical role for S5 helix Met-305 in voltage sensor to pore domain coupling. *Prog. Biophys. Mol. Biol.* **2021**, *166*, 156−172.
(189) Tong, J.-J.; Khan, U.; Haddad, B. G.; Minogue, P. J.; Beyer, E. C.; Berthoud, V. M.; Reichow, S. L.; Ebihara, L. Molecular mechanisms underlying enhanced hemichannel function of a cataract-associated Cx50 mutant. *Biophys. J.* **2021**, *120* (24), 5644−5656.
(190) Mukherjee, S.; Cassini, T. A.; Hu, N.; Yang, T.; Li, B.; Shen, W.; Moth, C. W.; Rinker, D. C.; Sheehan, J. H.; Cogan, J. D.; Newman, J. H.; Hamid, R.; Macdonald, R. L.; Roden, D. M.; Meiler, J.; Kuenze, G.; Phillips, J. A.; Capra, J. A. Personalized structural biology reveals the molecular mechanisms underlying heterogeneous epileptic phenotypes caused by de novo KCNC2 variants. *Hum. Genet. Genomics Adv.* **2022**, *3* (4), 100131.
(191) Llanos, M. A.; Ventura, C.; Martín, P.; Enrique, N.; Felice, J. I.; Gavernet, L.; Milesi, V. Novel Dimeric hHv1Model and Structural Bioinformatic Analysis Reveal an ATP-Binding Site Resulting in a Channel Activating Effect. *J. Chem. Inf. Model.* **2022**, *62* (13), 3200−3212.
(192) Wang, P.; Gao, X.; Zhang, K.; Pei, Q.; Xu, X.; Yan, F.; Dong, J.; Jing, C. Exploring the binding mechanism of positive allosteric modulators in human metabotropic glutamate receptor 2 using molecular dynamics simulations. *Phys. Chem. Chem. Phys.* **2021**, *23* (42), 24125−24139.
(193) Yin, Y.; Zhang, F.; Feng, S.; Butay, K. J.; Borgnia, M. J.; Im, W.; Lee, S.-Y. Activation mechanism of the mouse cold-sensing TRPM8 channel by cooling agonist and PIP_2. *Science* **2022**, *378* (6616), eadd1268.
(194) Feng, S.; Pumroy, R. A.; Protopopova, A. D.; Moiseenkova-Bell, V. Y.; Im, W. Modulation of TRPV2 by Endogenous and Exogenous Ligands: A Computational Study. *Protein Sci.* **2023**, *32*, e4490.
(195) Mernea, M.; Ulăreanu, R. Ş.; Cucu, D.; Al-Saedi, J. H.; Pop, C.-E.; Fendrihan, S.; Anghelescu, G. D. C.; Mihăilescu, D. F. Epithelial Sodium Channel Inhibition by Amiloride Addressed with THz Spectroscopy and Molecular Modeling. *Molecules* **2022**, *27* (10), 3271.
(196) Cali, E.; Dominik, N.; Manole, A.; Houlden, H. Riboflavin Transporter Deficiency. In *GeneReviews*; Adam, M. P., E, D., Mirzaa,

https://doi.org/10.1021/acs.jctc.2c01246
J. Chem. Theory Comput. 2023, 19, 2161−2185

G. M., Pagon, R. A., Wallace, S. E., LJH, Bean, Gripp, K. W., Amemiya, A, Eds.; University of Washington, Seattle: Seattle, WA, 2015.
(197) Yahyaoui, R.; Pérez-Frías, J. Amino Acid Transport Defects in Human Inherited Metabolic Disorders. *Int. J. Mol. Sci.* **2020**, *21* (1), 119.
(198) Chen, Z.; Shi, T.; Zhang, L.; Zhu, P.; Deng, M.; Huang, C.; Hu, T.; Jiang, L.; Li, J. Mammalian drug efflux transporters of the ATP binding cassette (ABC) family in multidrug resistance: A review of the past decade. *Cancer Lett.* **2016**, *370* (1), 153−164.
(199) Malinverni, J. C.; Silhavy, T. J. An ABC transport system that maintains lipid asymmetry in the Gram-negative outer membrane. *Proc. Natl. Acad. Sci. U. S. A.* **2009**, *106* (19), 8009−8014.
(200) Sperandeo, P.; Martorana, A. M.; Polissi, A. The lipopolysaccharide transport (Lpt) machinery: A nonconventional transporter for lipopolysaccharide assembly at the outer membrane of Gram-negative bacteria. *J. Biol. Chem.* **2017**, *292* (44), 17981−17990.
(201) Choi, U. Antimicrobial Agents That Inhibit the Outer Membrane Assembly Machines of Gram-Negative Bacteria. *J. Microbiol. Biotechnol.* **2019**, *29* (1), 1−10.
(202) Alexander, S. P. H.; Kelly, E.; Mathie, A.; Peters, J. A.; Veale, E. L.; Armstrong, J. F.; Faccenda, E.; Harding, S. D.; Pawson, A. J.; Southan, C.; Davies, J. A.; Amarosi, L.; Anderson, C. M. H.; Beart, P. M.; Broer, S.; Dawson, P. A.; Hagenbuch, B.; Hammond, J. R.; Hancox, J. C.; Inui, K.-i.; Kanai, Y.; Kemp, S.; Stewart, G.; Thwaites, D. T.; Verri, T. THE CONCISE GUIDE TO PHARMACOLOGY 2021/22: Transporters. *Br. J. Pharmacol.* **2021**, *178* (S1), S412−S513.
(203) Raturi, S.; Nair, A. V.; Shinoda, K.; Singh, H.; Bai, B.; Murakami, S.; Fujitani, H.; van Veen, H. W. Engineered MATE multidrug transporters reveal two functionally distinct ion-coupling pathways in NorM from Vibrio cholerae. *Commun. Biol.* **2021**, *4* (1), 558.
(204) Zhao, J.; Xie, H.; Mehdipour, A. R.; Safarian, S.; Ermler, U.; Münke, C.; Thielmann, Y.; Hummer, G.; Ebersberger, I.; Wang, J.; Michel, H. The structure of the *Aquifex aeolicus* MATE family multidrug resistance transporter and sequence comparisons suggest the existence of a new subfamily. *Proc. Natl. Acad. Sci. U. S. A.* **2021**, *118* (46), e2107335118.
(205) Bavnhøj, L.; Paulsen, P. A.; Flores-Canales, J. C.; Schiøtt, B.; Pedersen, B. P. Molecular mechanism of sugar transport in plants unveiled by structures of glucose/H^+ symporter STP10. *Nature Plants* **2021**, *7* (10), 1409−1419.
(206) Han, M.; Chen, L. Y. Molecular dynamics simulation of human urea transporter B. *Mol. Simul.* **2021**, *47* (12), 1022−1028.
(207) Prescher, M.; Bonus, M.; Stindt, J.; Keitel-Anselmino, V.; Smits, S. H. J.; Gohlke, H.; Schmitt, L. Evidence for a credit-card-swipe mechanism in the human PC floppase ABCB4. *Structure* **2021**, *29* (10), 1144−1155.e5.
(208) Li, C.; Yue, Z.; Newstead, S.; Voth, G. A. Proton coupling and the multiscale kinetic mechanism of a peptide transporter. *Biophys. J.* **2022**, *121* (12), 2266−2278.
(209) Weigle, A. T.; Carr, M.; Shukla, D. Impact of Increased Membrane Realism on Conformational Sampling of Proteins. *J. Chem. Theory Comput.* **2021**, *17* (8), 5342−5357.
(210) Adil, M. T.; Rahman, R.; Whitelaw, D.; Jain, V.; Al-Taan, O.; Rashid, F.; Munasinghe, A.; Jambulingam, P. SARS-CoV-2 and the pandemic of COVID-19. *Postgrad. Med. J.* **2021**, *97* (1144), 110.
(211) Simon, V.; Ho, D. D.; Abdool Karim, Q. HIV/AIDS epidemiology, pathogenesis, prevention, and treatment. *Lancet* **2006**, *368* (9534), 489−504.
(212) El-Kamary, S. S.; Kottilil, S. 35 - Viral Hepatitis. In *Hunter's Tropical Medicine and Emerging Infectious Diseases*, 10th ed.; Ryan, E. T., Hill, D. R., Solomon, T., Aronson, N. E., Endy, T. P., Eds.; Elsevier: London, 2020; pp 308−324.
(213) Hasan, S.; Ahmad, S. A.; Masood, R.; Saeed, S. Ebola virus: A global public health menace: A narrative review. *J. Family Med. Prim. Care* **2019**, *8* (7), 2189.
(214) Villalaín, J. Envelope E protein of dengue virus and phospholipid binding to the late endosomal membrane. *Biochim. Biophys. Acta, Biomembr.* **2022**, *1864* (5), 183889.
(215) Monje-Galvan, V.; Voth, G. A. Molecular interactions of the M and E integral membrane proteins of SARS-CoV-2. *Faraday Discuss.* **2021**, *232* (0), 49−67.
(216) Norris, M. J.; Husby, M. L.; Kiosses, W. B.; Yin, J.; Saxena, R.; Rennick, L. J.; Heiner, A.; Harkins, S. S.; Pokhrel, R.; Schendel, S. L.; Hastie, K. M.; Landeras-Bueno, S.; Salie, Z. L.; Lee, B.; Chapagain, P. P.; Maisner, A.; Duprex, W. P.; Stahelin, R. V.; Saphire, E. O. Measles and Nipah virus assembly: Specific lipid binding drives matrix polymerization. *Sci. Adv.* **2022**, *8* (29), eabn1440.
(217) Woo, H.; Park, S.-J.; Choi, Y. K.; Park, T.; Tanveer, M.; Cao, Y.; Kern, N. R.; Lee, J.; Yeom, M. S.; Croll, T. I.; Seok, C.; Im, W. Developing a Fully Glycosylated Full-Length SARS-CoV-2 Spike Protein Model in a Viral Membrane. *J. Phys. Chem. B* **2020**, *124* (33), 7128−7137.
(218) Cao, Y.; Choi, Y. K.; Frank, M.; Woo, H.; Park, S.-J.; Yeom, M. S.; Seok, C.; Im, W. Dynamic Interactions of Fully Glycosylated SARS-CoV-2 Spike Protein with Various Antibodies. *J. Chem. Theory Comput.* **2021**, *17* (10), 6559−6569.
(219) Kim, S.; Liu, Y.; Ziarnik, M.; Seo, S.; Cao, Y.; Zhang, X. F.; Im, W. Binding of human ACE2 and RBD of Omicron enhanced by unique interaction patterns among SARS-CoV-2 variants of concern. *J. Comput. Chem.* **2023**, *44*, 594.
(220) Kim, S.; Liu, Y.; Lei, Z.; Dicker, J.; Cao, Y.; Zhang, X. F.; Im, W. Differential Interactions between Human ACE2 and Spike RBD of SARS-CoV-2 Variants of Concern. *J. Chem. Theory Comput.* **2021**, *17* (12), 7972−7979.
(221) Jacquemard, C.; Koensgen, F.; Colin, P.; Lagane, B.; Kellenberger, E. Modeling of CCR5 Recognition by HIV-1 gp120: How the Viral Protein Exploits the Conformational Plasticity of the Coreceptor. *Viruses* **2021**, *13* (7), 1395.
(222) Ramazi, S.; Mohammadi, N.; Allahverdi, A.; Khalili, E.; Abdolmaleki, P. A review on antimicrobial peptides databases and the computational tools. *Database* **2022**, *2022*, baac011.
(223) Boparai, K. J.; Sharma, K. P. Mini Review on Antimicrobial Peptides, Sources, Mechanism and Recent Applications. *Protein Pept. Lett.* **2019**, *27* (1), 4−16.
(224) Miyazaki, Y.; Shinoda, W. Cooperative antimicrobial action of melittin on lipid membranes: A coarse-grained molecular dynamics study. *Biochim. Biophys. Acta, Biomembr.* **2022**, *1864* (9), 183955.
(225) Herrera-León, C.; Ramos-Martín, F.; El Btaouri, H.; Antonietti, V.; Sonnet, P.; Martiny, L.; Zevolini, F.; Falciani, C.; Sarazin, C.; D'Amelio, N. The Influence of Short Motifs on the Anticancer Activity of HB43 Peptide. *Pharmaceutics* **2022**, *14* (5), 1089.
(226) Almeida, C. V.; de Oliveira, C. F. R.; dos Santos, E. L.; dos Santos, H. F.; Júnior, E. C.; Marchetto, R.; da Cruz, L. A.; Ferreira, A. M. T.; Gomes, V. M.; Taveira, G. B.; Costa, B. O.; Franco, O. L.; Cardoso, M. H.; Macedo, M. L. R. Differential interactions of the antimicrobial peptide, RQ18, with phospholipids and cholesterol modulate its selectivity for microorganism membranes. *Biochim. Biophys. Acta, Gen. Subj.* **2021**, *1865* (9), 129937.
(227) Bierbaum, G.; Sahl, H. G. Lantibiotics: Mode of Action, Biosynthesis and Bioengineering. *Curr. Pharm. Biotechnol.* **2009**, *10* (1), 2−18.
(228) Pokhrel, R.; Bhattarai, N.; Baral, P.; Gerstman, B. S.; Park, J. H.; Handfield, M.; Chapagain, P. P. Lipid II Binding and Transmembrane Properties of Various Antimicrobial Lanthipeptides. *J. Chem. Theory Comput.* **2022**, *18* (1), 516−525.
(229) Gaza, J. T.; Leyson, J. J. C.; Peña, G. T.; Nellas, R. B. pH-Dependent Conformations of an Antimicrobial Spider Venom Peptide, Cupiennin 1a, from Unbiased HREMD Simulations. *ACS Omega* **2021**, *6* (37), 24166−24175.
(230) Karmakar, S.; Klauda, J. B. Modeling the membrane binding mechanism of a lipid transport protein Osh4 to single membranes. *Biophys. J.* **2022**, *121* (8), 1560−1575.

(231) Rubel, M. S.; Fedotov, S. A.; Grizel, A. V.; Sopova, J. V.; Malikova, O. A.; Chernoff, Y. O.; Rubel, A. A. Functional Mammalian Amyloids and Amyloid-Like Proteins. *Life* **2020**, *10* (9), 156.
(232) Zhang, D. Y.; Wang, J.; Fleeman, R. M.; Kuhn, M. K.; Swulius, M. T.; Proctor, E. A.; Dokholyan, N. V. Monosialotetrahexosylganglioside Promotes Early Aβ42 Oligomer Formation and Maintenance. *ACS Chem. Neurosci.* **2022**, *13* (13), 1979−1991.
(233) Garten, M.; Prévost, C.; Cadart, C.; Gautier, R.; Bousset, L.; Melki, R.; Bassereau, P.; Vanni, S. Methyl-branched lipids promote the membrane adsorption of α-synuclein by enhancing shallow lipid-packing defects. *Phys. Chem. Chem. Phys.* **2015**, *17* (24), 15589−15597.
(234) Espinosa, Y. R.; Barrera Valderrama, D. I.; Carlevaro, C. M.; Llanos, E. J. Molecular basis of the anchoring and stabilization of human islet amyloid polypeptide in lipid hydroperoxidized bilayers. *Biochim. Biophys. Acta, Gen. Subj.* **2022**, *1866* (10), 130200.
(235) Pal, T.; Paul, R.; Paul, S. Phenylpropanoids on the Inhibition of β-Amyloid Aggregation and the Movement of These Molecules through the POPC Lipid Bilayer. *Langmuir* **2022**, *38* (25), 7775−7790.
(236) Monje-Galvan, V.; Klauda, J. B. Peripheral membrane proteins: Tying the knot between experiment and computation. *Biochim. Biophys. Acta, Biomembr.* **2016**, *1858* (7, Part B), 1584−1593.
(237) Boes, D. M.; Godoy-Hernandez, A.; McMillan, D. G. G. Peripheral Membrane Proteins: Promising Therapeutic Targets across Domains of Life. *Membranes* **2021**, *11* (5), 346.
(238) Schulz, T. A.; Prinz, W. A. Sterol transport in yeast and the oxysterol binding protein homologue (OSH) family. *Biochim. Biophys. Acta, Mol. Cell Biol. Lipids* **2007**, *1771* (6), 769−780.
(239) Raychaudhuri, S.; Im, Y. J.; Hurley, J. H.; Prinz, W. A. Nonvesicular sterol movement from plasma membrane to ER requires oxysterol-binding protein−related proteins and phosphoinositides. *J. Cell Biol.* **2006**, *173* (1), 107−119.
(240) Aleshin, A. E.; Yao, Y.; Iftikhar, A.; Bobkov, A. A.; Yu, J.; Cadwell, G.; Klein, M. G.; Dong, C.; Bankston, L. A.; Liddington, R. C.; Im, W.; Powis, G.; Marassi, F. M. Structural basis for the association of PLEKHA7 with membrane-embedded phosphatidylinositol lipids. *Structure* **2021**, *29* (9), 1029−1039.e3.
(241) Friday, B. B.; Adjei, A. A. K-ras as a target for cancer therapy. *Biochim. Biophys. Acta, Rev. Cancer* **2005**, *1756* (2), 127−144.
(242) Lu, H.; Martí, J. Predicting the conformational variability of oncogenic GTP-bound G12D mutated KRas-4B proteins at zwitterionic model cell membranes. *Nanoscale* **2022**, *14* (8), 3148−3158.
(243) Bos, M. P.; Robert, V.; Tommassen, J. Biogenesis of the Gram-Negative Bacterial Outer Membrane. *Annu. Rev. Microbiol.* **2007**, *61* (1), 191−214.
(244) Pang, Z.; Raudonis, R.; Glick, B. R.; Lin, T.-J.; Cheng, Z. Antibiotic resistance in *Pseudomonas aeruginosa*: mechanisms and alternative therapeutic strategies. *Biotechnol. Adv.* **2019**, *37* (1), 177−192.
(245) Edrington, T. C.; Kintz, E.; Goldberg, J. B.; Tamm, L. K. Structural Basis for the Interaction of Lipopolysaccharide with Outer Membrane Protein H (OprH) from *Pseudomonas aeruginosa**. *J. Biol. Chem.* **2011**, *286* (45), 39211−39223.
(246) Rosenhouse-Dantsker, A.; Mehta, D.; Levitan, I. Regulation of Ion Channels by Membrane Lipids. *Compr. Physiol.* **2012**, *2*, 31−68.
(247) Sarkar, P.; Chattopadhyay, A. Cholesterol in GPCR Structures: Prevalence and Relevance. *J. Membr. Biol.* **2022**, *255* (1), 99−106.
(248) Di Scala, C.; Baier, C. J.; Evans, L. S.; Williamson, P. T. F.; Fantini, J.; Barrantes, F. J. Chapter One - Relevance of CARC and CRAC Cholesterol-Recognition Motifs in the Nicotinic Acetylcholine Receptor and Other Membrane-Bound Receptors. In *Current Topics in Membranes*; Levitan, I., Ed.; Academic Press: 2017; Vol. *80*, pp 3−23.
(249) Hanson, M. A.; Cherezov, V.; Griffith, M. T.; Roth, C. B.; Jaakola, V.-P.; Chien, E. Y. T.; Velasquez, J.; Kuhn, P.; Stevens, R. C. A Specific Cholesterol Binding Site Is Established by the 2.8 Å Structure of the Human β2-Adrenergic Receptor. *Structure* **2008**, *16* (6), 897−905.
(250) Corradi, V.; Bukiya, A. N.; Miranda, W. E.; Cui, M.; Plant, L. D.; Logothetis, D. E.; Tieleman, D. P.; Noskov, S. Y.; Rosenhouse-Dantsker, A. A molecular switch controls the impact of cholesterol on a Kir channel. *Proc. Natl. Acad. Sci. U. S. A.* **2022**, *119* (13), e2109431119.
(251) Song, W.; Corey, R. A.; Ansell, T. B.; Cassidy, C. K.; Horrell, M. R.; Duncan, A. L.; Stansfeld, P. J.; Sansom, M. S. P. PyLipID: A Python Package for Analysis of Protein−Lipid Interactions from Molecular Dynamics Simulations. *J. Chem. Theory Comput.* **2022**, *18* (2), 1188−1201.
(252) Taghon, G. J.; Rowe, J. B.; Kapolka, N. J.; Isom, D. G. Predictable cholesterol binding sites in GPCRs lack consensus motifs. *Structure* **2021**, *29* (5), 499−506.e3.
(253) Kjølbye, L. R.; Sørensen, L.; Yan, J.; Berglund, N. A.; Ferkinghoff-Borg, J.; Robinson, C. V.; Schiøtt, B. Lipid Modulation of a Class B GPCR: Elucidating the Modulatory Role of PI(4,5)P_2 Lipids. *J. Chem. Inf. Model.* **2022**, *62*, 6788.
(254) Martens, C.; Shekhar, M.; Borysik, A. J.; Lau, A. M.; Reading, E.; Tajkhorshid, E.; Booth, P. J.; Politis, A. Direct protein-lipid interactions shape the conformational landscape of secondary transporters. *Nat. Commun.* **2018**, *9* (1), 4151.
(255) Mandal, K. Review of PIP2 in Cellular Signaling, Functions and Diseases. *Int. J. Mol. Sci.* **2020**, *21* (21), 8342.
(256) Claveras Cabezudo, A.; Feriel Khoualdi, A.; D'Avanzo, N. Computational Prediction of Phosphoinositide Binding to Hyperpolarization-Activated Cyclic-Nucleotide Gated Channels. *Front. Physiol.* **2022**, *13*, 859087.
(257) Belovich, A. N.; Aguilar, J. I.; Mabry, S. J.; Cheng, M. H.; Zanella, D.; Hamilton, P. J.; Stanislowski, D. J.; Shekar, A.; Foster, J. D.; Bahar, I.; Matthies, H. J. G.; Galli, A. A network of phosphatidylinositol (4,5)-bisphosphate (PIP_2) binding sites on the dopamine transporter regulates amphetamine behavior in Drosophila Melanogaster. *Mol. Psychiatry* **2021**, *26* (8), 4417−4430.
(258) Wu, E. L.; Qi, Y.; Song, K. C.; Klauda, J. B.; Im, W. Preferred Orientations of Phosphoinositides in Bilayers and Their Implications in Protein Recognition Mechanisms. *J. Phys. Chem. B* **2014**, *118* (16), 4315−4325.
(259) Hansen, S. B.; Tao, X.; MacKinnon, R. Structural basis of PIP_2 activation of the classical inward rectifier K^+ channel Kir2.2. *Nature* **2011**, *477* (7365), 495−498.
(260) Duncan, A. L.; Corey, R. A.; Sansom, M. S. P. Defining how multiple lipid species interact with inward rectifier potassium (Kir2) channels. *Proc. Natl. Acad. Sci. U. S. A.* **2020**, *117* (14), 7803−7813.
(261) Lee, J.; Cha, S.-K.; Sun, T.-J.; Huang, C.-L. PIP_2 Activates TRPV5 and Releases Its Inhibition by Intracellular Mg^{2+}. *J. Gen. Physiol.* **2005**, *126* (5), 439−451.
(262) Ufret-Vincenty, C. A.; Klein, R. M.; Hua, L.; Angueyra, J.; Gordon, S. E. Localization of the PIP2 Sensor of TRPV1 Ion Channels*. *J. Biol. Chem.* **2011**, *286* (11), 9688−9698.
(263) Choi, H.-K.; Kang, H.; Lee, C.; Kim, H. G.; Phillips, B. P.; Park, S.; Tumescheit, C.; Kim, S. A.; Lee, H.; Roh, S.-H.; Hong, H.; Steinegger, M.; Im, W.; Miller, E. A.; Choi, H.-J.; Yoon, T.-Y. Evolutionary balance between foldability and functionality of a glucose transporter. *Nat. Chem. Biol.* **2022**, *18* (7), 713−723.
(264) Neale, C.; Herce, H. D.; Pomès, R.; García, A. E. Can Specific Protein-Lipid Interactions Stabilize an Active State of the Beta 2 Adrenergic Receptor? *Biophys. J.* **2015**, *109* (8), 1652−1662.
(265) Manglik, A.; Kim, T. H.; Masureel, M.; Altenbach, C.; Yang, Z.; Hilger, D.; Lerch, M. T.; Kobilka, Tong S.; Thian, Foon S.; Hubbell, Wayne L.; Prosser, R. S.; Kobilka, Brian K. Structural Insights into the Dynamic Process of β2-Adrenergic Receptor Signaling. *Cell* **2015**, *161* (5), 1101−1111.
(266) Horvath, S. E.; Daum, G. Lipids of mitochondria. *Prog. Lipid Res.* **2013**, *52* (4), 590−614.

https://doi.org/10.1021/acs.jctc.2c01246
J. Chem. Theory Comput. 2023, 19, 2161−2185

(267) Yi, Q.; Yao, S.; Ma, B.; Cang, X. The effects of cardiolipin on the structural dynamics of the mitochondrial ADP/ATP carrier in its cytosol-open state. *J. Lipid Res.* **2022**, *63* (6), 100227.
(268) Di Meo, F.; Fabre, G.; Berka, K.; Ossman, T.; Chantemargue, B.; Paloncýová, M.; Marquet, P.; Otyepka, M.; Trouillas, P. In silico pharmacology: Drug membrane partitioning and crossing. *Pharmacol. Res.* **2016**, *111*, 471−486.
(269) Atanasov, A. G.; Zotchev, S. B.; Dirsch, V. M.; Orhan, I. E.; Banach, M.; Rollinger, J. M.; Barreca, D.; Weckwerth, W.; Bauer, R.; Bayer, E. A.; Majeed, M.; Bishayee, A.; Bochkov, V.; Bonn, G. K.; Braidy, N.; Bucar, F.; Cifuentes, A.; D'Onofrio, G.; Bodkin, M.; Diederich, M.; Dinkova-Kostova, A. T.; Efferth, T.; El Bairi, K.; Arkells, N.; Fan, T.-P.; Fiebich, B. L.; Freissmuth, M.; Georgiev, M. I.; Gibbons, S.; Godfrey, K. M.; Gruber, C. W.; Heer, J.; Huber, L. A.; Ibanez, E.; Kijjoa, A.; Kiss, A. K.; Lu, A.; Macias, F. A.; Miller, M. J. S.; Mocan, A.; Müller, R.; Nicoletti, F.; Perry, G.; Pittalà, V.; Rastrelli, L.; Ristow, M.; Russo, G. L.; Silva, A. S.; Schuster, D.; Sheridan, H.; Skalicka-Woźniak, K.; Skaltsounis, L.; Sobarzo-Sánchez, E.; Bredt, D. S.; Stuppner, H.; Sureda, A.; Tzvetkov, N. T.; Vacca, R. A.; Aggarwal, B. B.; Battino, M.; Giampieri, F.; Wink, M.; Wolfender, J.-L.; Xiao, J.; Yeung, A. W. K.; Lizard, G.; Popp, M. A.; Heinrich, M.; Berindan-Neagoe, I.; Stadler, M.; Daglia, M.; Verpoorte, R.; Supuran, C. T.; the International Natural Product Sciences, T.; et al. Natural products in drug discovery: advances and opportunities. *Nat. Rev. Drug Discov.* **2021**, *20* (3), 200−216.
(270) Hewlings, S. J.; Kalman, D. S. Curcumin: A Review of Its Effects on Human Health. *Foods* **2017**, *6* (10), 92.
(271) Lyu, Y.; Xiang, N.; Mondal, J.; Zhu, X.; Narsimhan, G. Characterization of Interactions between Curcumin and Different Types of Lipid Bilayers by Molecular Dynamics Simulation. *J. Phys. Chem. B* **2018**, *122* (8), 2341−2354.
(272) Nguyen, T. Q. T.; Lund, F. W.; Zanjani, A. A. H.; Khandelia, H. Magic mushroom extracts in lipid membranes. *Biochim. Biophys. Acta, Biomembr.* **2022**, *1864* (9), 183957.
(273) Cheeseman, S.; Elbourne, A.; Gangadoo, S.; Shaw, Z. L.; Bryant, S. J.; Syed, N.; Dickey, M. D.; Higgins, M. J.; Vasilev, K.; McConville, C. F.; Christofferson, A. J.; Crawford, R. J.; Daeneke, T.; Chapman, J.; Truong, V. K. Interactions between Liquid Metal Droplets and Bacterial, Fungal, and Mammalian Cells. *Adv. Mater. Interfaces* **2022**, *9* (7), 2102113.
(274) Shobhna; Kumari, M.; Kashyap, H. K. Mechanistic Insight on BioIL-Induced Structural Alterations in DMPC Lipid Bilayer. *J. Phys. Chem. B* **2021**, *125* (43), 11955−11966.
(275) Siani, P.; Donadoni, E.; Ferraro, L.; Re, F.; Di Valentin, C. Molecular dynamics simulations of doxorubicin in sphingomyelin-based lipid membranes. *Biochim. Biophys. Acta, Biomembr.* **2022**, *1864* (1), 183763.
(276) Winslow, M.; Robinson, D. Computational development of a phase-sensitive membrane raft probe. *Phys. Chem. Chem. Phys.* **2022**, *24* (14), 8260−8268.
(277) Sessa, L.; Concilio, S.; Di Martino, M.; Nardiello, A. M.; Miele, Y.; Rossi, F.; Brunetti, J.; Panunzi, B.; Piotto, S. A selective Nile Red based solvatochromic probe: A study of fluorescence in LUVs and GUVs model membranes. *Dyes Pigm.* **2021**, *196*, 109759.
(278) Li, J.; Kalyanram, P.; Rozati, S.; Monje-Galvan, V.; Gupta, A. Interaction of Cyanine-D112 with Binary Lipid Mixtures: Molecular Dynamics Simulation and Differential Scanning Calorimetry Study. *ACS Omega* **2022**, *7* (11), 9765−9774.
(279) Lei, Z.; Chen, B.; Koo, Y. M.; MacFarlane, D. R. Introduction: Ionic Liquids. *Chem. Rev.* **2017**, *117* (10), 6633−6635.
(280) Kneiszl, R.; Hossain, S.; Larsson, P. In Silico-Based Experiments on Mechanistic Interactions between Several Intestinal Permeation Enhancers with a Lipid Bilayer Model. *Mol. Pharm.* **2022**, *19* (1), 124−137.
(281) Song, W.; Joshi, H.; Chowdhury, R.; Najem, J. S.; Shen, Y.-x.; Lang, C.; Henderson, C. B.; Tu, Y.-M.; Farell, M.; Pitz, M. E.; Maranas, C. D.; Cremer, P. S.; Hickey, R. J.; Sarles, S. A.; Hou, J.-l.; Aksimentiev, A.; Kumar, M. Artificial water channels enable fast and selective water permeation through water-wire networks. *Nat. Nanotechnol.* **2020**, *15* (1), 73−79.
(282) Ebrahimi, M.; Foroutan, M. High-Performance Biomimetic Water Channel: The Constructive Interplay of Interaction Parameters and Hydrophilic Doping Levels. *J. Phys. Chem. B* **2021**, *125* (41), 11566−11581.
(283) Hardiagon, A.; Murail, S.; Huang, L.-B.; Lee, A. v. d.; Sterpone, F.; Barboiu, M.; Baaden, M. Molecular dynamics simulations reveal statistics and microscopic mechanisms of water permeation in membrane-embedded artificial water channel nano-constructs. *J. Chem. Phys.* **2021**, *154* (18), 184102.
(284) Muraoka, T.; Noguchi, D.; Kasai, R. S.; Sato, K.; Sasaki, R.; Tabata, K. V.; Ekimoto, T.; Ikeguchi, M.; Kamagata, K.; Hoshino, N.; Noji, H.; Akutagawa, T.; Ichimura, K.; Kinbara, K. A synthetic ion channel with anisotropic ligand response. *Nat. Commun.* **2020**, *11* (1), 2924.
(285) Miao, M.; Shao, X.; Cai, W. Conformational Change from U- to I-Shape of Ion Transporters Facilitates K^+ Transport across Lipid Bilayers. *J. Phys. Chem. B* **2022**, *126* (7), 1520−1528.
(286) Zhu, X.; Li, N.; Huang, C.; Li, Z.; Fan, J. Membrane Perturbation and Lipid Flip-Flop Mediated by Graphene Nanosheet. *J. Phys. Chem. B* **2020**, *124* (47), 10632−10640.
(287) Lolicato, F.; Joly, L.; Martinez-Seara, H.; Fragneto, G.; Scoppola, E.; Baldelli Bombelli, F.; Vattulainen, I.; Akola, J.; Maccarini, M. The Role of Temperature and Lipid Charge on Intake/Uptake of Cationic Gold Nanoparticles into Lipid Bilayers. *Small* **2019**, *15* (23), 1805046.
(288) Ganguly, P.; Breen, A.; Pillai, S. C. Toxicity of Nanomaterials: Exposure, Pathways, Assessment, and Recent Advances. *ACS Biomater. Sci. Eng.* **2018**, *4* (7), 2237−2275.
(289) Palit, S. H.; Chaudhery, M. Engineered nanomaterial for industrial use. In *Handbook of Nanomaterials for industrial applications*; Hussain, C. M., Ed.; Elsevier: Newark, NJ, United States.
(290) Bahadar, H.; Maqbool, F.; Niaz, K.; Abdollahi, M. Toxicity of Nanoparticles and an Overview of Current Experimental Models. *Iran. Biomed. J.* **2016**, *20* (1), 1−11.
(291) Murali, A.; Lokhande, G.; Deo, K. A.; Brokesh, A.; Gaharwar, A. K. Emerging 2D nanomaterials for biomedical applications. *Mater. Today* **2021**, *50*, 276−302.
(292) Plachá, D.; Jampilek, J. Graphenic Materials for Biomedical Applications. *Nanomaterials* **2019**, *9* (12), 1758.
(293) Jeevanandam, J.; Barhoum, A.; Chan, Y. S.; Dufresne, A.; Danquah, M. K. Review on nanoparticles and nanostructured materials: history, sources, toxicity and regulations. *Beilstein J. Nanotechnol.* **2018**, *9*, 1050−1074.
(294) Contini, C.; Schneemilch, M.; Gaisford, S.; Quirke, N. Nanoparticle−membrane interactions. *J. Exp. Nanosci.* **2018**, *13* (1), 62−81.
(295) Foreman-Ortiz, I. U.; Liang, D.; Laudadio, E. D.; Calderin, J. D.; Wu, M.; Keshri, P.; Zhang, X.; Schwartz, M. P.; Hamers, R. J.; Rotello, V. M.; Murphy, C. J.; Cui, Q.; Pedersen, J. A. Anionic nanoparticle-induced perturbation to phospholipid membranes affects ion channel function. *Proc. Natl. Acad. Sci. U. S. A.* **2020**, *117* (45), 27854−27861.
(296) Pantelopulos, G. A.; Nagai, T.; Bandara, A.; Panahi, A.; Straub, J. E. Critical size dependence of domain formation observed in coarse-grained simulations of bilayers composed of ternary lipid mixtures. *J. Chem. Phys.* **2017**, *147* (9), No. 095101.
(297) Rice, A.; Haldar, S.; Wang, E.; Blank, P. S.; Akimov, S. A.; Galimzyanov, T. R.; Pastor, R. W.; Zimmerberg, J. Planar aggregation of the influenza viral fusion peptide alters membrane structure and hydration, promoting poration. *Nat. Commun.* **2022**, *13* (1), 7336.
(298) Beaven, A. H.; Maer, A. M.; Sodt, A. J.; Rui, H.; Pastor, R. W.; Andersen, O. S.; Im, W. Gramicidin A Channel Formation Induces Local Lipid Redistribution I: Experiment and Simulation. *Biophys. J.* **2017**, *112* (6), 1185−1197.
(299) Hajeyah, A. A.; Griffiths, W. J.; Wang, Y.; Finch, A. J.; O'Donnell, V. B. The Biosynthesis of Enzymatically Oxidized Lipids. *Front. Endocrinol.* **2020**, *11*, 591819.

(300) Zingg, J.-M.; Vlad, A.; Ricciarelli, R. Oxidized LDLs as Signaling Molecules. *Antioxidants* **2021**, *10* (8), 1184.
(301) Tsubone, T. M.; Junqueira, H. C.; Baptista, M. S.; Itri, R. Contrasting roles of oxidized lipids in modulating membrane microdomains. *Biochim. Biophys. Acta, Biomembr.* **2019**, *1861* (3), 660−669.
(302) Cosma, C. L.; Sherman, D.R.; Ramakrishnan, L. The Secret Lives of the Pathogenic Mycobacteria. *Annu. Rev. Microbiol.* **2003**, *57* (1), 641−676.
(303) Dulberger, C. L.; Rubin, E. J.; Boutte, C. C. The mycobacterial cell envelope — a moving target. *Nat. Rev. Microbiol.* **2020**, *18* (1), 47−59.
(304) Dufourc, E. J. Bicelles and nanodiscs for biophysical chemistry. *Biochim. Biophys. Acta, Biomembr.* **2021**, *1863* (1), 183478.
(305) Rani, G.; Kuroda, K.; Vemparala, S. Towards designing globular antimicrobial peptide mimics: role of polar functional groups in biomimetic ternary antimicrobial polymers. *Soft Matter* **2021**, *17* (8), 2090−2103.
(306) Magalhães, R. P.; Fernandes, H. S.; Sousa, S. F. Modelling Enzymatic Mechanisms with QM/MM Approaches: Current Status and Future Challenges. *Isr. J. Chem.* **2020**, *60* (7), 655−666.
(307) Rattu, P.; Glencross, F.; Mader, S. L.; Skylaris, C.-K.; Matthews, S. J.; Rouse, S. L.; Khalid, S. Atomistic level characterisation of ssDNA translocation through the E. coli proteins CsgG and CsgF for nanopore sequencing. *Comput. Struct. Biotechnol. J.* **2021**, *19*, 6417−6430.
(308) Rózsa, Z. B.; Németh, L. J.; Jójárt, B.; Nehéz, K.; Viskolcz, B.; Szőri, M. Molecular Dynamics and Metadynamics Insights of 1,4-Dioxane-Induced Structural Changes of Biomembrane Models. *J. Phys. Chem. B* **2019**, *123* (37), 7869−7884.

https://doi.org/10.1021/acs.jctc.2c01246
J. Chem. Theory Comput. 2023, 19, 2161−2185